Cell Reports

Article

A lncRNA-mediated metabolic rewiring of cell senescence

Graphical abstract

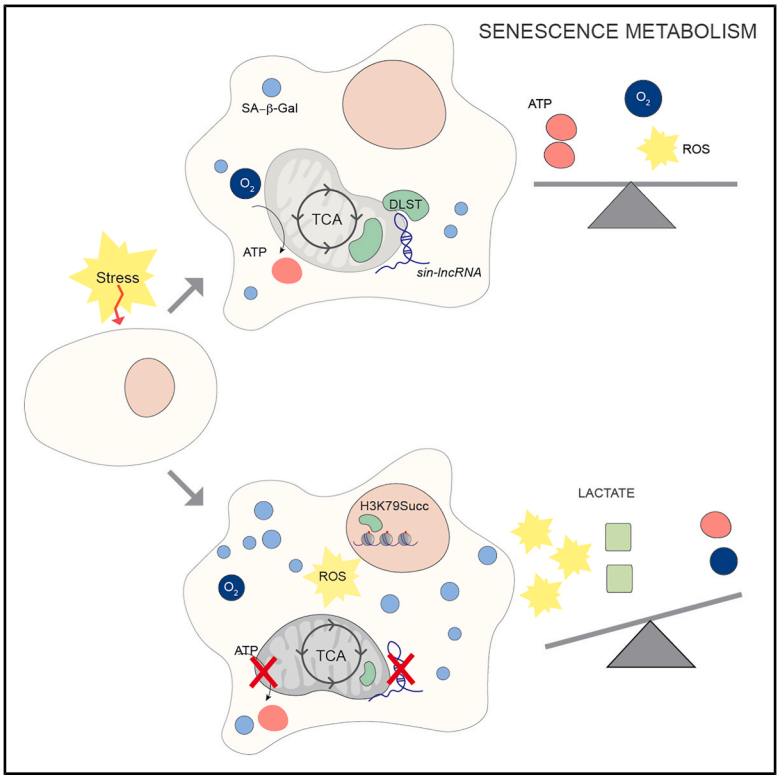

Highlights

- *sin-lncRNA* is specifically induced by CEBPβ in senescence
- *sin-lncRNA* interacts with DLST to maintain its mitochondrial localization
- DLST translocates to the nucleus upon *sin-lncRNA* depletion, altering mitochondrial function
- Nuclear translocation of DLST leads to transcriptional changes in metabolic genes

Authors

Elena Grossi, Francesco P. Marchese, Jovanna González, ..., Leonor Puchades-Carrasco, Marta Montes, Maite Huarte

Correspondence

mmontesr@unav.es (M.M.), maitehuarte@unav.es (M.H.)

In brief

Grossi et al. describe how *sin-lncRNA* interacts with the TCA enzyme DLST to maintain mitochondrial function and metabolic balance during senescence. Depletion of *sin-lncRNA* causes DLST translocation to the nucleus, impairing mitochondrial function and triggering transcriptional changes, leading to metabolic reprogramming in senescence.

Grossi et al., 2025, Cell Reports *44*, 115747
June 24, 2025 © 2025 The Author(s). Published by Elsevier Inc.
https://doi.org/10.1016/j.celrep.2025.115747

CellPress

Cell Reports

CellPress
OPEN ACCESS

Article

A lncRNA-mediated metabolic rewiring of cell senescence

Elena Grossi,[1,2,6,7] Francesco P. Marchese,[1,2] Jovanna González,[1,2] Enrique Goñi,[1,2] José Miguel Fernández-Justel,[1,2] Alicia Amadoz,[1,2] Nicolás Herranz,[3,4] Leonor Puchades-Carrasco,[5] Marta Montes,[1,2,*] and Maite Huarte[1,2,8,*]

[1]Center for Applied Medical Research, University of Navarra, Pamplona, Spain
[2]Institute of Health Research of Navarra (IdiSNA), Pamplona, Spain
[3]Vall d'Hebron Institute of Oncology (VHIO), Barcelona, Spain
[4]Vall d'Hebron Institute of Research (VHIR), Barcelona, Spain
[5]Drug Discovery Unit, Instituto de Investigación Sanitaria La Fe (IISLAFE), 46026 Valencia, Spain
[6]Present address: Departments of Oncological Sciences and Dermatology, Icahn School of Medicine at Mount Sinai, New York, NY, USA
[7]Present address: Tisch Cancer Institute, Icahn School of Medicine at Mount Sinai, New York, NY, USA
[8]Lead contact
*Correspondence: mmontesr@unav.es (M.M.), maitehuarte@unav.es (M.H.)
https://doi.org/10.1016/j.celrep.2025.115747

SUMMARY

Despite not proliferating, senescent cells remain metabolically active to maintain the senescence program. However, the mechanisms behind this metabolic reprogramming are not well understood. We identify senescence-induced long noncoding RNA (*sin-lncRNA*), a previously uncharacterized long noncoding RNA (lncRNA), a key player in this response. While strongly activated in senescence by C/EBPβ, *sin-lncRNA* loss reinforces the senescence program by altering oxidative phosphorylation and rewiring mitochondrial metabolism. By interacting with dihydrolipoamide S-succinyltransferase (DLST), it facilitates its mitochondrial localization. Depletion of *sin-lncRNA* causes DLST nuclear translocation, leading to transcriptional changes in oxidative phosphorylation (OXPHOS) genes. While not expressed in highly proliferative cancer cells, it is strongly induced upon cisplatin-induced senescence. Depletion of *sin-lncRNA* in ovarian cancer cells reduces oxygen consumption and increases extracellular acidification, sensitizing cells to cisplatin treatment. Altogether, these results indicate that *sin-lncRNA* is specifically induced in senescence to maintain metabolic homeostasis, unveiling an RNA-dependent metabolic rewiring specific to senescent cells.

INTRODUCTION

Senescence is a permanent state of growth arrest that can be induced by different types of stress, such as shortening of telomeres due to extensive replication, DNA damage, oxidative stress, chemotherapy treatment, or oncogene overexpression.[1] Senescent cells present characteristic morphological and biochemical features such as enlarged size, halted proliferation, activation of senescence-associated (SA) β-galactosidase activity, and increased expression of cell cycle inhibitors.[1] Furthermore, in several types of senescence, the cells secrete a combination of interleukins, metalloproteases, and growth factors, collectively known as the SA secretory phenotype (SASP).[2–4] While the SASP reinforces senescence, its chronic activation can have pro-tumorigenic effects and contribute to several aging-related pathologies.[5] In fact, the persistence of therapy-induced senescent cancer cells in the tumor has been linked to resistance to chemotherapy.[6,7] There is, therefore, a critical need to develop combinatorial approaches to not only stop proliferation but also induce the elimination of the senescent tumor cells.

Despite their decreased proliferative potential, senescent cells are metabolically active in order to cope with the energetic demands of the senescence program.[8] Indeed, metabolic reprogramming is considered a hallmark of senescence.[9] In general, senescent cells accumulate dysfunctional mitochondria resulting in an increase of reactive oxygen species (ROS).[10–12] Although different triggers of senescence result in broad metabolic differences, the interplay between senescent cells and metabolism is highly dynamic and context dependent, and the underlying mechanisms remain largely unexplored. In this context, long noncoding RNAs (lncRNAs) represent a relatively uncharted territory for investigation.

LncRNAs are transcripts recently defined as longer than 500 nucleotides with exquisite cell type-specific expression patterns that lack protein-coding potential.[13] They are tightly regulated during development or in response to signaling pathways.[14] Although it is still unclear how many of the thousands of annotated lncRNAs have a significant biological role, several have been found to be essential for the regulation of key cellular processes, such as proliferation and differentiation, as well as a broad range of diseases including cancer.[15,16] Notably, our previous work and other laboratories' have reported that specific lncRNAs are differentially expressed during senescence induction,[17,18] regulating multiple senescence aspects, from

This is an open access article under the CC BY-NC-ND license (http://creativecommons.org/licenses/by-nc-nd/4.0/).

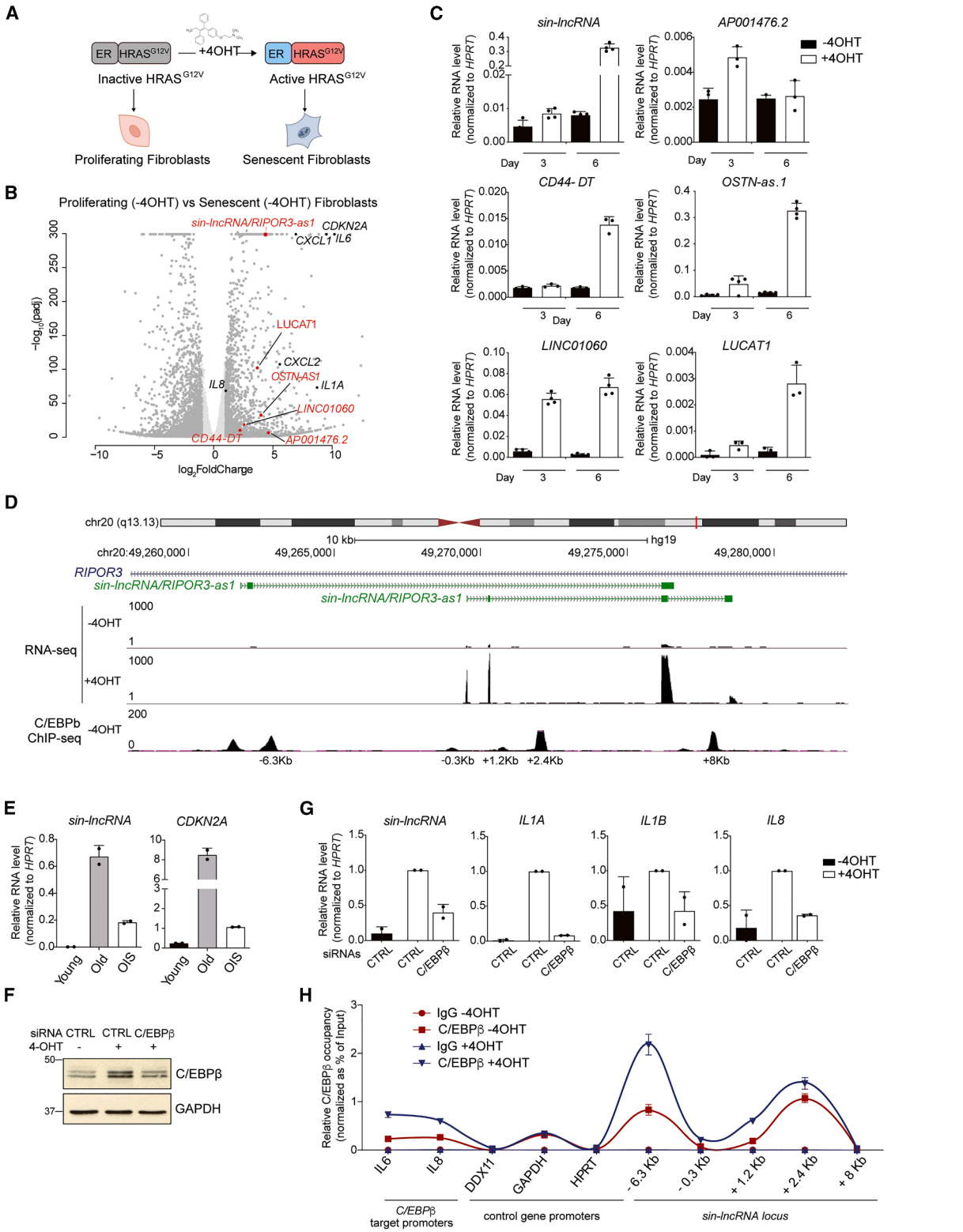

(legend on next page)

transcriptional response to SASP production.[19–22] Intriguingly, recent studies have involved a number of lncRNAs in the regulation of cellular metabolism,[23–26] and noncoding RNAs (ncRNAs) are emerging as interactors and regulators of metabolic enzymes.[27] However, the contribution of this functional diverse class of molecules to the metabolic reprogramming of senescent cells remains unknown.

Here, we report the identification of the senescence-specific lncRNA, senescence-induced lncRNA (*sin-lncRNA*), which is induced in senescence to prevent uncontrolled metabolic alterations, by regulating the function of a key metabolic enzyme and the transcription of metabolic genes. Together, our results provide evidence of an RNA-dependent metabolic rewiring specific to the senescent cellular state.

RESULTS

Oncogene-induced senescence leads to broad changes in gene expression, encompassing alterations in lncRNAs

Although the importance of lncRNAs in a variety of cellular processes is now fully recognized, only a handful of them have been described as directly implicated in cellular senescence. To identify novel regulators of this process, we analyzed RNA sequencing (RNA-seq) data from a cellular system that recapitulates senescence induction *in vitro* thanks to the controlled activation of an oncogene.[28] IMR90 non-immortalized lung fibroblasts were engineered to express an oncogenic HRAS variant ($HRAS^{G12V}$) fused to the estrogen receptor (ER:RAS), which is activated following 4-hydroxy-tamoxifen (4OHT) administration (Figure 1A).[3,29] Multiple senescence markers, such as arrest of proliferation and increased expression of pro-inflammatory factors and tumor suppressors, along with detectable β-galactosidase staining, were observed, ensuring proper senescence progression (Figures S1A–S1E). Furthermore, the presence of SA heterochromatin foci, as well as an increase in H3K9me3 and γH2AX foci, confirmed the chromatin remodeling linked to oncogene-induced senescence (OIS) (Figures S1F and S1G). RNA-seq data generated in this cell system[28] detected more than 4,720 genes differentially expressed upon induction of senescence (log2FC > 1; *p* adj. < 0.05), including not only many coding genes (3,456) but also lncRNAs (951) (Figures 1B and S1H). The majority of lncRNAs (62%) were downregulated, which might reflect cell cycle inhibition during senescence, whereas the remaining 38% of lncRNAs were upregulated. We focused our attention on lncRNAs highly induced upon OIS, as we speculated they might play a role in the senescence process, and we verified their upregulation at different time points of OIS progression (Figures 1C and S1I).

Interestingly, we observed a previously uncharacterized lncRNA (*ENSG00000234693*) as one of the most significantly and strongly upregulated genes, with an induction comparable to that of key senescence genes *CKN2A*, *CXCL1*, and *IL6* (Figure 1B; Table S1). We consequently renamed it *senescence-induced lncRNA* or *sin-lncRNA*. *sin-lncRNA* is an intronic lncRNA located in chromosome 20 and transcribed in the antisense orientation of the protein-coding gene *RIPOR3* (Figures 1D, S2A, and S2B). *sin-lncRNA* lacks coding potential (Figure S2C) and presents two poly-adenylated isoforms annotated by GENCODE (v.41): a longer one (638 nt), composed by three exons, and a shorter one (539 nt) of four exons. However, only the shorter isoform is expressed and highly upregulated upon 4OHT treatment in IMR90 fibroblasts, according to both sequencing data and quantitative reverse-transcription PCR (RT-qPCR) performed with different primer sets (Figures 1D and S2A). This observation was confirmed by absolute quantification by RT-qPCR, which showed that *sin-lncRNA* is lowly expressed in proliferating conditions with ∼9 copies per cell, while, upon senescence induction, the expression of its short isoform increases up to ∼86 copies (Figure S2D).

Interestingly, *sin-lncRNA* levels increased only at later stages of senescence (Figures 1C and S2A), prompting us to investigate whether its upregulation was dependent on the full activation of a senescence program or rather related to the induction of the HRAS oncogene in OIS. To this aim, we analyzed *sin-lncRNA* expression levels in different types of senescence, such as replicative senescence—achieved by prolonged culture of untransformed IMR90 fibroblasts—and senescence induced by ionizing radiation (γ-irradiation). In all the systems analyzed, *sin-lncRNA* expression was strongly induced in the senescent context, correlating with known senescence markers, such as *CDKN2A* and *IL6* (Figures 1E and S2E).

Due to the strong and highly specific *sin-lncRNA* induction in senescence, we speculated that senescence-specific factors

Figure 1. *sin-lncRNA* is a senescence-specific lncRNA transcriptionally induced by C/EBPβ

(A) Schematic representation of normal fibroblasts undergoing OIS upon 4OHT-mediated activation of an oncogenic form of HRAS.

(B) Volcano plot depicting differential gene expression data (GSE61130) comparing IMR90 ER:RAS proliferating and senescent cells. Cutoff for significance $\log_2$FC > ±1; adj. *p* value < 0.05. A selection of canonical senescence markers (in black) and lncRNAs (in red) is shown.

(C) RT-qPCR analysis of a set of lncRNA candidates upregulated upon 4OHT time course (3 or 6 days) in IMR90 ER:RAS cells; *RIPOR3-as1* was amplified with primer set#2 (see Figure S2A for details). Data are presented as mean values ± SD. *n* = 3/4.

(D) Genomic snapshot of *sin-lncRNA* locus with RNA-seq tracks of untreated and 4OHT-treated IMR90 ER:RAS fibroblasts, as well as C/EBPβ ChIP-seq ENCODE data generated in IMR90 cells.

(E) RT-qPCR analysis of "young" (<14 passages) and "old" (>30 passages) IMR90 fibroblasts and 4OHT-induced "OIS" IMR90 ER:RAS cells shows that *sin-lncRNA* upregulation is maintained in replicative senescence, compared to p16-positive control. (*n* = 2).

(F) Western blot analysis of control and C/EBPβ-depleted senescent IMR90 ER:RAS cells. Proliferating fibroblasts were used as further control.

(G) RT-qPCR analysis of *sin-lncRNA*, as well as a set of C/EBPβ target genes in control and C/EBPβ-depleted senescent IMR90 ER:RAS cells. Data are represented as mean values ± SD. (*n* = 2).

(H) ChIP-qPCR analysis of C/EBPβ in proliferating and senescent IMR90 ER:RAS cells upon 6 days of 4OHT treatment. IgG immunoprecipitation (IP) was used as IP control; C/EBPβ peaks at *sin-lncRNA* locus are labeled according to their distance from *sin-lncRNA* TSS; regions located in *DDX11*, *GAPDH*, and *HPRT* promoters served as negative controls, *IL6* and *IL8* promoter regions as positive controls (*n* = 2).

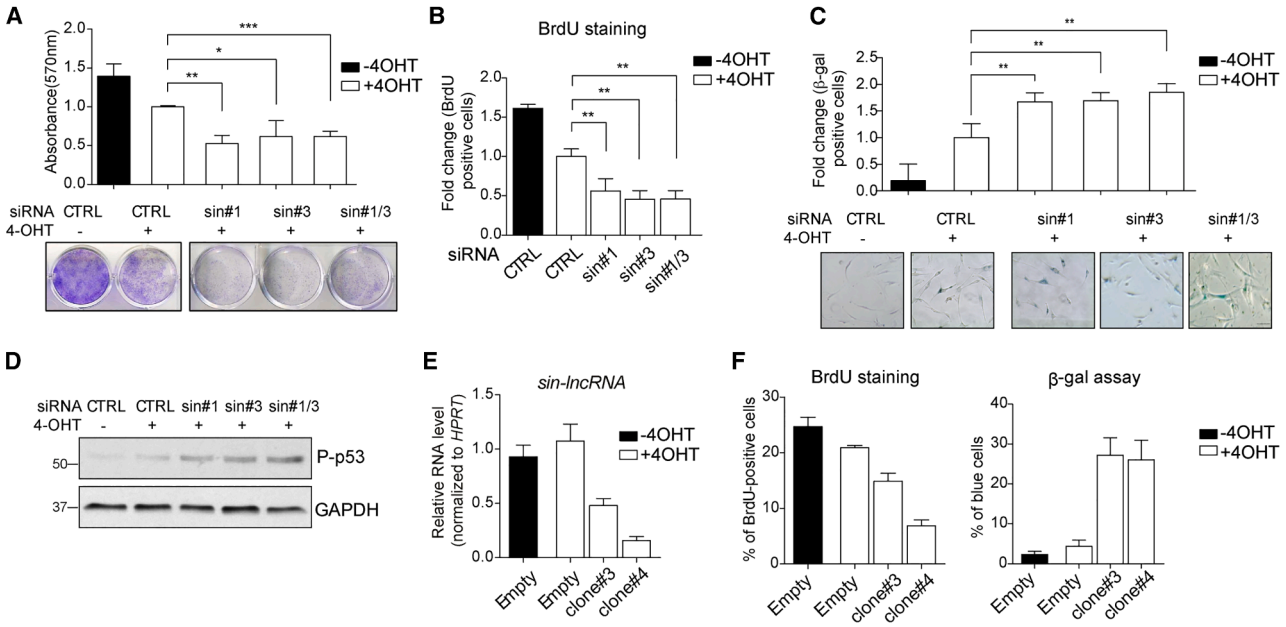

Figure 2. *sin-lncRNA* depletion reinforces the senescent phenotype

(A and B) (A) Crystal violet assay and (B) BrdU analysis assessing cell growth of control and *sin-lncRNA*-depleted IMR90 ER:RAS fibroblasts after 5 days of senescence induction. $^{*}p < 0.05$; $^{**}p < 0.01$; $^{***}p < 0.001$.

(C) β-galactosidase analysis of control and *sin-lncRNA*-depleted IMR90 cells induced to senescence for 8 days. Scale bars: 100 μm. $^{**}p < 0.01$.

(D) Western blot analysis of control and *sin-lncRNA*-depleted IMR90 cells treated with 4OHT for 5 days.

(E) RT-qPCR analysis of TIG3 BRAF cell clones infected with *sin-lncRNA* sgRNA or an empty plasmid.

(F) BrdU (left) and β-galactosidase (right) assays of control or *sin-lncRNA* sgRNA TIG3 BRAF clones.

could regulate the expression of this lncRNA. We took advantage of chromatin immunoprecipitation sequencing (ChIP-seq) data generated in IMR90[30] cells to examine the *sin-lncRNA* genomic region, finding that the transcription factor C/EBPβ was bound to several positions in the proximity of *sin-lncRNA* transcription start site (TSS) and gene body (Figure 1D). Interestingly, C/EBPβ exerts an important role in the later stages of senescence induction, mainly by activating genes related to inflammation and SASP.[31] After confirming the previously reported C/EBPβ upregulation in OIS[2] (Figure S2F), we depleted C/EBPβ in senescent cells and analyzed *sin-lncRNA* expression (Figures 1F, 1G, and S2G). Notably, the induction of *sin-lncRNA* in senescence was prevented by C/EBPβ depletion, similarly to what occurred with *IL1β*, *IL6*, and *IL8*, other canonical targets of this transcription factor (Figure 1G). To further investigate whether or not *sin-lncRNA* is a C/EBPβ transcriptional target, we performed ChIP-qPCR of this transcription factor in proliferative and senescent conditions (Figure 1H). C/EBPβ was found enriched at *sin-lncRNA* regulatory regions, and its binding increased in senescent cells (Figure 1H), supporting the evidence that the senescence driver C/EBPβ controls *sin-lncRNA* expression at later stages of senescence induction and suggesting that the lncRNA might exert a role in this response.

sin-lncRNA loss contributes to the senescent phenotype through increase of oxidative stress

To explore the function of *sin-lncRNA*, we depleted it in senescent IMR90 ER:RAS fibroblasts (Figure S3A) and analyzed several senescence markers at 5 days of induction to detect intermediate states before the cells enter a fully stable senescent phenotype.[32] Interestingly, *sin-lncRNA* knockdown further decreased the proliferation of senescent cells (Figures 2A, 2C, and S3B), increased the percentage of β-galactosidase-positive cells (Figure 2C), and activated the p53 signaling pathway (Figure 2D), without changing levels of apoptosis (Figure S3C), indicating that *sin-lncRNA* knockdown reinforces the senescent phenotype.

To investigate the broader significance of these results, we investigated other senescence systems and methods for *sin-lncRNA* loss of function. We took advantage of TIG3 hTERT lung fibroblasts engineered to express an inducible and constitutively active portion of the human BRAF oncogene to drive OIS (TIG3 BRAF:ER).[33] In this cell system, we again observed reduced proliferation upon *sin-lncRNA* downregulation by RNAi (Figures S3D–S3F), indicating that *sin-lncRNA* depletion leads to the same phenotype regardless of the type of oncogene expressed. We also generated TIG3 BRAF:ER cell lines stably depleted of *sin-lncRNA* by CRISPR-Cas9 technology. Despite not being able to isolate viable cell clones with *sin-lncRNA* biallelic deletion, we found that the removal of just one allele was sufficient to decrease *sin-lncRNA* expression, leading to a consistent strengthening of the senescence phenotype (Figures 2E, 2F, S3G, and S3H). Altogether, these results suggest that the loss of *sin-lncRNA* reinforces the induction of cellular senescence.

To investigate which aspect of the complex senescence response is influenced by *sin-lncRNA*, we analyzed the global

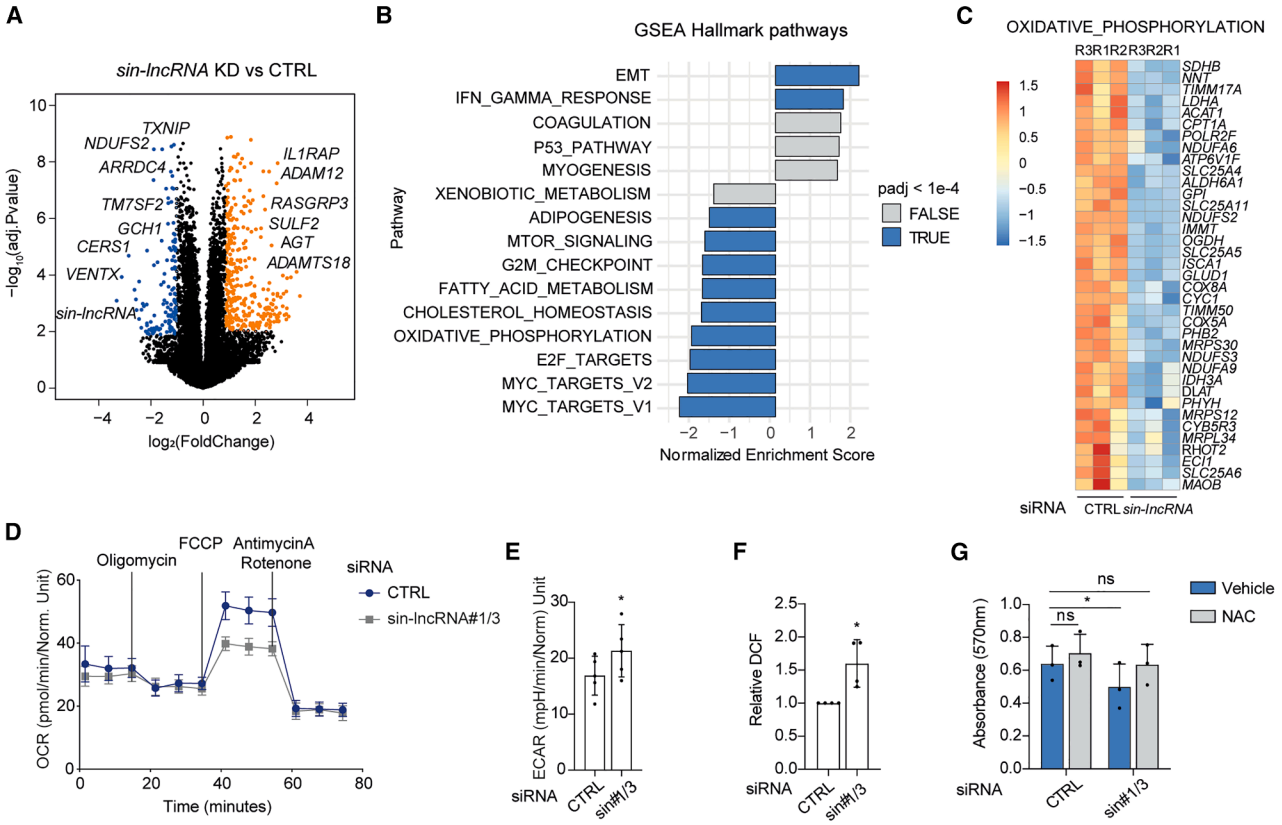

Figure 3. *sin-lncRNA* knockdown alters oxidative stress response and metabolic pathways in senescent cells

(A) Volcano plot depicting differentially expressed genes comparing *sin-lncRNA* knockdown vs. control IMR90 ER:RAS senescent cells. Upregulated genes (adj. p value < 0.01; log2FC > 1) are labeled in red, downregulated genes (adj. p value < 0.01; log2FC < −1) in blue.

(B) Hallmark gene set enrichment analysis (GSEA) reporting the most enriched pathways associated to the genes differentially expressed (DE) upon *sin-lncRNA* depletion (threshold: adj. p value < 1e−4).

(C) Heatmap highlighting expression changes across RNA-seq replicates of genes belonging to OXIDATIVE_PHOSPHORILATION GSEA pathway.

(D) Oxygen consumption rate (OCR) of control or *sin-lncRNA*-depleted IMR90 ER:RAS senescent cells obtained using the Seahorse XFe96 Analyzer following injections of oligomycin, FCCP, and rotenone/antimycin A, as indicated. Data are presented as mean ± SD (n = 4). Two-way ANOVA and Sidak's multiple comparisons test, *p < 0.05.

(E) Basal extracellular acidification rate (ECAR) measured using the Seahorse XFe96 analyzer, in the same conditions as in (D), and following injections of glucose, oligomycin, and 2-deoxy-D-glucose, as indicated in the glycolysis stress test. Data are presented as mean ± SD (n = 4). Two-tailed student's t test, *p < 0.05.

(F) Fluorometric analysis measuring the amount of the fluorescent oxidized probe 2′,7′-dichlorofluorescein (DCF), as indicative of ROS/NOS intracellular levels in control and *sin-lncRNA*-depleted IMR90 ER:RAS fibroblasts induced to senescence for 5 days. Proliferating control cells were used as further control.

(G) Absorbance levels of crystal violet solution measured at 560 nm from vehicle or N-acetyl-L-cysteine (NAC)-treated IMR90 ER:RAS fibroblasts transfected with siRNA control (CTRL) or against *sin-lncRNA* (sin#1/3) and induced to senescence for 5 days. The graph represents the mean ± SD (n = 3). Two-tailed Student's t test, *p < 0.05.

changes in gene expression by RNA-seq of *sin-lncRNA*-depleted ER:RAS fibroblasts upon senescence induction (Figures 3A and S4A; Table S2) and employed gene set enrichment analysis to determine enriched pathways associated with the observed changes in gene expression (Figures 3B and S4B). Interestingly, among the most significantly reduced terms were several metabolic pathways, such as cholesterol homeostasis and fatty acid (FA) metabolism. Moreover, mRNAs belonging to oxidative phosphorylation pathway were significantly downregulated, including the mitochondrial ADP/ATP carrier (AAC) 1, 2, and 3 (*SLC25A4*, *SLC25A5*, and *SLC25A6*, respectively), which regulate key transport steps for cellular ATP production[34] (Figures 3B and 3C).

Since metabolic rearrangements and altered oxidative phosphorylation (OXPHOS) are known to be linked to senescence,[13,35] we speculated that *sin-lncRNA* could influence the metabolic states of senescent cells. To analyze metabolic alterations upon *sin-lncRNA* depletion, we measured the oxygen consumption rate coupled to ATP production during OXPHOS by Seahorse assay.[36] Compared to control senescent cells, *sin-lncRNA* knockdown led to the reduction of several key parameters of mitochondrial function, most significantly impacting maximal respiration rate, mitochondrial spare capacity, and coupling efficiency (Figures 3D and S4C). We also observed an increment in extracellular acidification rate (ECAR) in *sin-lncRNA*-depleted cells, a reflection of increased aerobic

glycolysis that has been linked to defects in ATP production[37] (Figure 3E).

Since alterations in OXPHOS are also linked to increased oxidative stress,[38–40] we measured intracellular levels of reactive oxygen and nitrogen species and observed a significant enrichment of oxidant species in *sin-lncRNA*-depleted senescent ER:RAS cells (Figure 3F), suggesting that *sin-lncRNA* is involved in the control of oxidative stress in senescent cells. The increase in oxidant species and metabolic dysfunctions can reinforce senescence.[41,42] We therefore hypothesized that *sin-lncRNA* depletion might exacerbate senescence-related mitochondrial alteration and promote oxidative stress, thereby leading to the observed senescence reinforcement. Indeed, blocking ROS accumulation by N-acetyl-L-cysteine treatment[43,44] restored cell growth and reduced SA-β-galactosidase activation in senescent cells depleted for *sin-lncRNA* (Figures 3G and S4D). Together, these data support the notion that *sin-lncRNA* contributes to manage the metabolic rewiring and oxidative stress response of senescent cells.

sin-lncRNA interacts with DLST and controls its subcellular localization

LncRNAs have been previously associated with defects in oxidative stress and metabolic pathways, in particular in cancer, where they alter gene programs through different mechanisms.[19,45] To elucidate how *sin-lncRNA* regulates the metabolic response of senescent cells, we first analyzed *sin-lncRNA* subcellular localization by RNA fluorescence *in situ* hybridization (FISH) and found it to be mainly enriched in the cytoplasm of senescent fibroblasts (Figures 4A and S5A). Interestingly, an independent study[46] indicated that *sin-lncRNA* is enriched in the mitoplasts of senescent cells (Figure S5B). We purified mitochondria from senescent cells by fluorescence-activated cell sorting (FACS) and detected the presence of *sin-lncRNA* along with mitochondrially encoded transcripts (Figures 4B and S5C). Together, these data suggest that *sin-lncRNA* acts in the mitochondria to control proliferative and metabolic pathways of senescent cells.

Reasoning that *sin-lncRNA* function could be mediated through interacting proteins, we set to unbiasedly identify its protein partners by RNA pull-down. We incubated *in vitro* transcribed *sin-lncRNA* or an unrelated control RNA with senescent IMR90 ER:RAS extracts and isolated interacting proteins (method details) (Figure S5D). Mass spectrometry (MS) revealed several proteins enriched (>2 unique peptides) specifically associated with *sin-lncRNA* but not with the control RNA (Figure S5E; Table S3). Notably, the most abundant proteins retrieved by MS analysis were dihydrolipoamide S-succinyltransferase (DLST) and DEAD-box helicase 28 (DDX28), which localize in the mitochondria and have a recognized role in that compartment,[47] in line with our findings linking *sin-lncRNA* to senescent cell metabolism.

DLST, identified as the main *sin-lncRNA* interactor, is the E2 component of the α-ketoglutarate dehydrogenase complex (KGDH), which is essential for the entry of glutamine into the tricarboxylic acid (TCA) cycle[48] (Figure 4C). DLST has been recently identified as an RNA-binding protein in an RNA-binding screen.[49] We orthogonally confirmed the interaction between the endogenous *sin-lncRNA* and DLST by RNA immunoprecipitation in senescent fibroblasts (Figures 4D and S5F), suggesting that they are functionally related. In order to map the region of *sin-lncRNA* interacting with DLST, we performed an *in vitro* pull-down with biotinylated fragments spanning the 539 nt of the full-length transcript. We observed that all fragments except F1 (1–150 nt) are involved in the binding (Figure S5G).

We then sought to investigate whether *sin-lncRNA* would regulate DLST expression or stability. However, DLST mRNA and protein levels were not affected upon *sin-lncRNA* knockdown and remained stable upon senescence induction (Figures S5H and S5I), indicating that neither *sin-lncRNA* nor cellular senescence modulates DLST expression. Of note, DLST is a protein that shuttles between different subcellular compartments. While its main activity takes place in the mitochondria, it is also localized in the nucleus, where it is known to regulate gene expression.[50–52] We therefore investigated whether DLST localization might be regulated by the lncRNA. Interestingly, cellular fractionation of senescent cells upon *sin-lncRNA* depletion showed that DLST levels were significantly decreased in the cytoplasm and increased in the nuclear fraction of cells (Figure 4E) in contrast to control senescence conditions (Figure S5J), suggesting that *sin-lncRNA* controls the subcellular localization of the metabolic enzyme DLST.

sin-lncRNA rewires metabolic activity in senescent cells

Given the change of DLST localization observed upon *sin-lncRNA* depletion, we sought to compare the phenotype of DLST depletion with the phenotypic alterations observed upon *sin-lncRNA* knockdown in senescent cells, as previous reports demonstrated increased ROS production upon DLST knockdown.[53] DLST knockdown in senescent fibroblasts led to an increase in the percentage of β-galactosidase-positive cells and decreased cell growth (Figures 5A and 5B), thus phenocopying *sin-lncRNA* knockdown in this regard. Deeper analysis of metabolic alterations showed an increase in lactate secretion in both *sin-lncRNA* and DLST-depleted senescent cells compared to control cells (Figure 5C), probably as a result of higher glycolytic activity in these cells (Figure 3C).

We further investigated the role of *sin-lncRNA* in metabolism by comparing changes in the levels of glutamine-derived metabolites upon *sin-lncRNA* and DLST knockdown in senescent cells using liquid chromatography-mass spectrometry (LC-MS) and fully labeled [U-^{13}C] glutamine as a tracer (Figure 5D). The glutamine-labeled fraction in cells grown with [U-^{13}C] glutamine consisted of >90% M+5 glutamine in all conditions, demonstrating equal incorporation of the labeled substrate (Figure S6A). While DLST knockdown strongly affected the TCA cycle, by decreasing the rate of glutamine oxidative metabolism, depletion of *sin-lncRNA* did not alter either oxidative or reductive TCA cycle activity (Figures S6A and S6B; Table S4). These results indicate that depletion of *sin-lncRNA* does not fully reproduce the metabolic effects of the knockdown of DLST, as expected, based on the protein relocalization caused by *sin-lncRNA* downregulation.

We hypothesized that, upon *sin-lncRNA* knockdown, alternative mechanisms might intervene to maintain a metabolic balance and compensate for deficiencies in KGDH complex

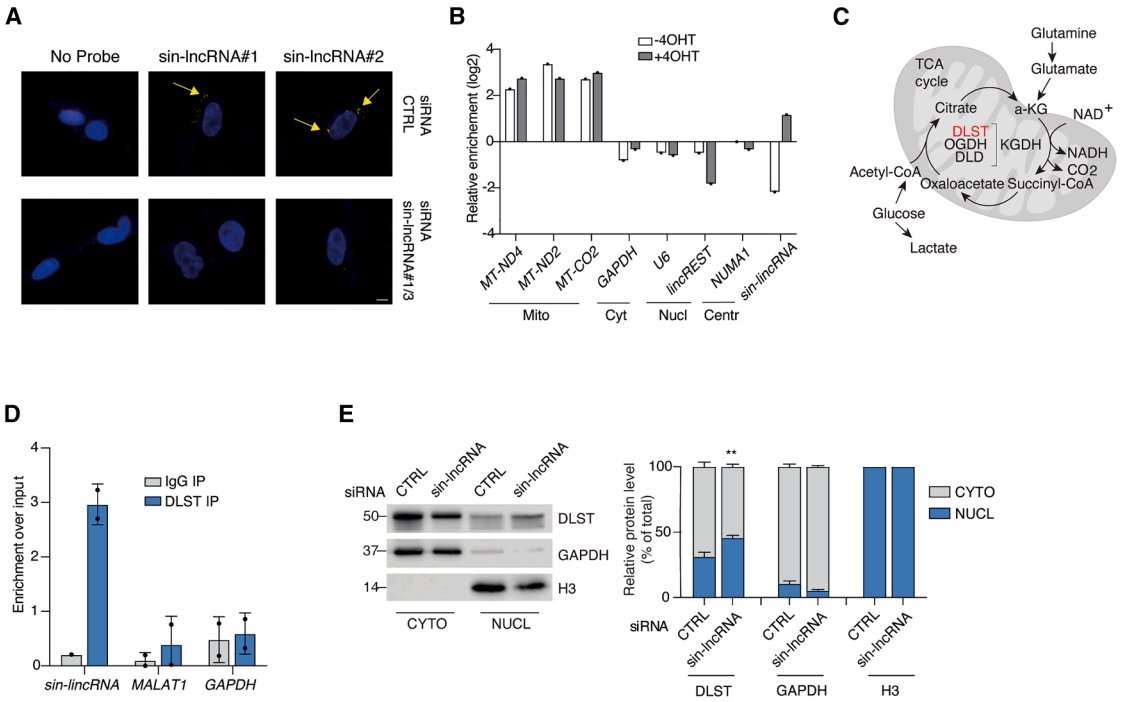

Figure 4. *sin-lncRNA* interacts with DLST and controls its subcellular localization

(A) RNA-FISH based on locked nucleic acid (LNA) technology on fixed IMR90 ER:RAS cells depleted or not of *sin-lncRNA* (siRNA_sin-lncRNA#1/3) and treated for 5 days with 4OHT. Two different LNAs were used. Incubation without LNA probe ("No_probe") was used as control. Scale bar: 10 μm.

(B) RT-qPCR analysis of a set of genes after mitochondria purification from proliferating (−4OHT) or senescent cells (+4OHT) using Mitotracker (green, 488) staining and FACS sorter. The graph shows a representative experiment.

(C) Schematic representation of the TCA cycle that takes place in the mitochondria. DLST enzyme is highlighted in red.

(D) RNA immunoprecipitation analysis monitoring DLST binding to *sin-lncRNA, MALAT1*, and *GAPDH* RNA in control and *sin-lncRNA*-depleted (siRNA#1/3) senescent IMR90 ER:RAS, using anti-DLST antibody or IgG as a negative control. The graph represents the mean ± SD ($n = 2$).

(E) Left, western blot analysis of DLST cellular fractionation in control and *sin-lncRNA*-depleted (siRNA#1/3) senescent IMR90 ER:RAS. GAPDH and H3 were used as cytoplasmic and nuclear controls, respectively. Right, percentage of nuclear and cytoplasmic distribution of DLST normalized to GAPDH (cyto) or H3 (nucl). The graph represents the mean ± SD ($n = 3$). Two-tailed Student's t test, $^{**}p < 0.01$.

activity. In agreement with this idea, the expression levels of the main enzymes implicated in the GABA shunt, an alternative route for the conversion of glutamate to succinate bypassing the TCA cycle,[54] were upregulated in *sin-lncRNA* knockdown cells (Figure 5D). We thus reasoned that the lack of the lncRNA resulted in a phenotypic output consequence of the decrease of DLST mitochondrial levels combined with events driven by increased nuclear levels of the protein.

DLST harbors a nuclear localization signal (NLS) that allows its translocation to the nucleus promoting the succinylation of H3K79.[52] Of note, we observed a significant overlap between mRNAs regulated by *sin-lncRNA* and genes regulated by KGDH-mediated H3K79 succinylation according to a prior study[52] (Figure S6C). We therefore investigated if DLST translocation could be involved in the observed transcriptional changes. Interestingly, overexpression of the wild-type DLST in senescent cells decreased the transcription of a subset of metabolic mRNAs, mimicking the effect of the depletion of *sin-lncRNA* (Figures 5E, S6E, and S6F). In contrast, a mutant DLST that is not able to enter the nucleus (R224A/K226E)[52] had no effect (Figure 5E). In fact, a previous study showed that relevant metabolic genes present H3K79Succ chromatin mark[52] (Figure S6D). Strikingly, we observed that H3K79Succ increased on these genes upon *sin-lncRNA* depletion in senescent cells, correlating with an increase in nuclear DLST (Figure 5F). These results show that the nuclear form, but not the cytoplasmic form, of DLST was able to reproduce the gene expression changes observed upon depletion of *sin-lncRNA*, supporting that the nuclear shuttling of DLST causes compensatory transcriptional changes observed in *sin-lncRNA* knockdown condition.

sin-lncRNA regulates OXPHOS in ovarian cancer cells

Our results indicate that *sin-lncRNA* is a regulator of the metabolic state of the senescent cells. To gain insight into the potential significance of *sin-lncRNA* function in a physio-pathological context, we interrogated gene expression data of tumor samples available through The Cancer Genome Atlas. *sin-lncRNA* presented low expression across cancer types (Figure S7A), and its expression negatively correlated with that of genes involved in active cell division, such as cyclins, as *CCNA2*, and members of the origin replication complex, such as *ORC1* and *MCM6*[55] (Figure S7B). Accordingly, terms related to cell cycle and mitosis were the most enriched Gene Ontology pathways associated

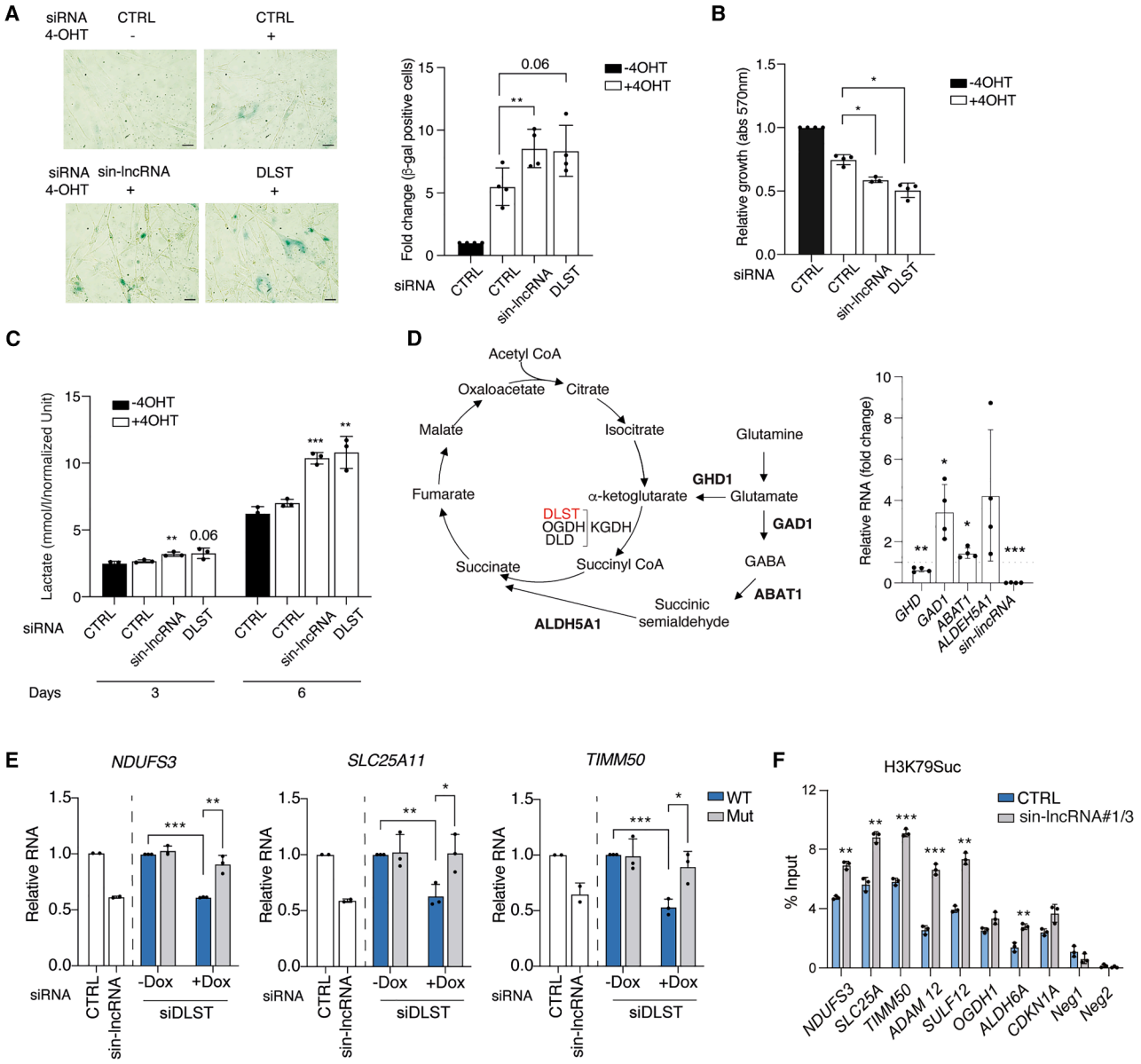

Figure 5. *sin-lncRNA* rewires metabolic activity in senescent cells

(A) Left, representative β-galactosidase images of untreated control cells and control, *sin-lncRNA*-depleted or DLST-depleted IMR90 cells induced to senescence for 5 days. Scale bars: 50 μm. Right, quantification of the percentage of β-galactosidase-positive cells in each condition normalized to control untreated cells set as 1. The graph represents the mean ± SD (n = 4). Two-tailed Student's t test, $^{**}p < 0.01$.

(B) Absorbance levels of crystal violet solution measured at 560 nm in the conditions described in (E). The graph represents the mean ± SD (n = 4). Two-tailed Student's t test, $^{*}p < 0.05$.

(C) Lactate levels measured from the supernatant of IMR90 ER:RAS fibroblasts transfected with the indicated siRNA and induced with 4OHT for 3 or 6 days. The graph represents the mean ± SD (n = 3). Two-tailed Student's t test, $^{*}p < 0.05$; $^{**}p < 0.01$; $^{***}p < 0.001$.

(D) Left, schematic showing alternative metabolic pathways. Right, RT-qPCR of the corresponding transcripts in sin-lncRNA knockdown cells relative to control (n = 3). The graph represents the mean ± SD (n = 4). Two-tailed Student's t test, $^{*}p < 0.05$; $^{**}p < 0.01$; $^{***}p < 0.001$.

(E) RT-qPCR of metabolic transcripts in the cells in stable senescent IMR90 ER:RAS cells expressing a doxycycline-inducible wild-type (WT) or NLS mutant (Mut) (R224A/K226E) DLST construct in the absence (−Dox) or presence (+Dox) of 100 ng/mL of doxycycline for 72 h (n = 3).

(F) ChIP-qPCR analysis of H3K79 succinylation in senescent IMR90 ER:RAS cells upon 6 days of 4OHT treatment transfected with siRNA control or siRNA against *sin-lncRNA* at the promoters of different metabolic genes. Regions located at intergenic regions (Neg1 and Neg2) served as negative controls. The graph shows a representative experiment (n = 2).

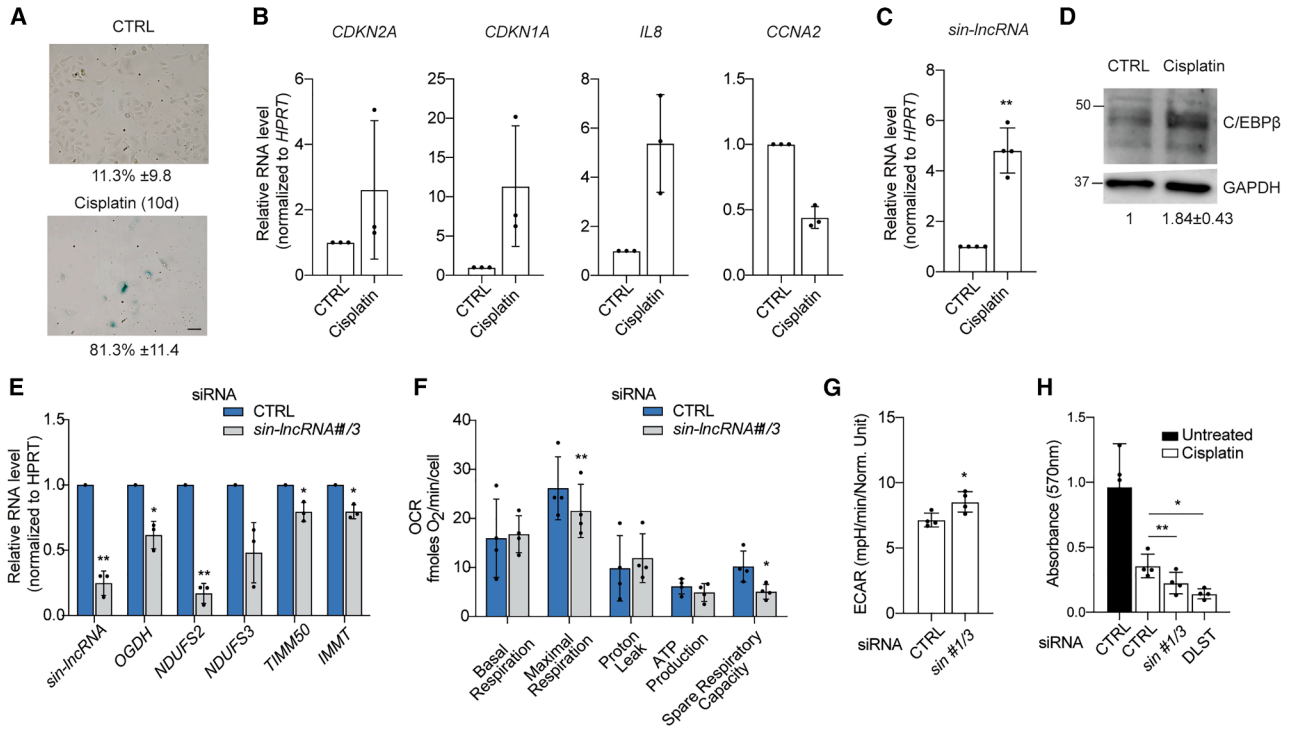

Figure 6. *sin-lncRNA* regulates OXPHOS in ovarian cancer cells

(A) Representative β-galactosidase images of untreated COV362 cells (upper) or treated for 10 days with μM cisplatin. Scale bars: 50 μm. Numbers represent the mean ± SD (n = 3).

(B) RT-qPCR analysis of senescence markers genes in cisplatin-treated COV362 for 10 days compared to untreated controls (set as 1).

(C) RT-qPCR analysis of *sin-lncRNA* in the cells described in (B). The graph represents the mean ± SD (n = 4). One sample t test, $^{**}p < 0.01$.

(D) Western blot analysis of C/EBPβ protein levels in the cells described in (B). Numbers represent the mean ± SD (n = 3).

(E) RT-qPCR analysis of OXPHOS GSEA pathway genes in control and *sin-lncRNA*-depleted (siRNA#1/3) COV362 senescent cells treated with cisplatin for 10 days.

(F) Oxygen consumption rate (OCR) of control or *sin-lncRNA*-depleted (siRNA#1/3) senescent COV362 cells obtained using the Seahorse XFe96 Analyzer following injections of oligomycin, FCCP, and rotenone/antimycin A, as indicated in the Cell Mito Stress Test. Data are presented as mean ± SD (n = 4). Two-tailed Student's t test, $^{*}p < 0.05$; $^{**}p < 0.01$.

(G) Basal extracellular acidification rate (ECAR) measured using the Seahorse XFe96 Analyzer, in the same conditions as in (F), and following injections of glucose, oligomycin, and 2-deoxy-D-glucose, as indicated in the glycolysis stress test. Data are presented as mean ± SD (n = 4). Two-tailed Student's t test, $^{*}p < 0.05$.

(H) Absorbance levels of crystal violet solution measured at 560 nm in proliferating or senescent COV362 cells transfected with control, *sin-lncRNA*, or DLST siRNA treated for 10 days with 10 μM cisplatin. $^{*}p < 0.05$; $^{**}p < 0.01$.

with these genes (Figure S7C). Since all these cell division-related genes presented a negative correlation with the senescence-specific *sin-lncRNA*, we speculated that a high expression of this noncoding transcript would predict cells with arrested cell cycle (e.g., senescent/quiescent cells), in line with the upregulation of *sin-lncRNA* upon OIS.

While tumor cells are highly proliferative, it has been shown that chemotherapy can induce cellular senescence, which can be linked to the resistance to treatment.[7] To investigate the potential significance of *sin-lncRNA* in response to cancer therapy, we analyzed the expression of the lncRNA in cisplatin-treated ovarian cancer cells, given their ability to undergo senescence upon treatment with platinum-based agents.[56] 10 days after cisplatin treatment, COV362 cells displayed a fully senescent phenotype, as confirmed by the expression of senescence markers, such as β-galactosidase, and the induction of cell cycle inhibitors and SASP components (Figures 6A and 6B). Interestingly, we observed a strong increase of *sin-lncRNA* expression in the senescent cells, whereas it was undetectable in untreated cells (Figure 6C). Cisplatin treatment also upregulated C/EBPβ expression (Figure 6D), suggesting that, also in the cancer cells, this transcription factor is responsible for the transcriptional activation of *sin-lncRNA*. As previously shown for senescent fibroblasts, knockdown of *sin-lncRNA* in cisplatin-treated COV362 cells reduced the expression of mRNAs involved in the OXPHOS pathway (Figure 6E), which was reflected in alterations in metabolic functions, such as decreased maximal respiration and increased ECAR (Figures 6F and 6G). Moreover, knockdown of either *sin-lncRNA* or DLST further decreased cell growth compared to control senescent cells (Figure 6H), indicating that depletion of the senescence-specific lncRNA sensitizes ovarian cancer senescent cells to cisplatin treatment.

Altogether, these data provide evidence that a lncRNA uniquely expressed in senescent cells contributes to the configuration of their metabolic state, also when senescence is

induced in cancer cells, thus representing a valuable marker and potential target in aging and cancer.

DISCUSSION

Although senescence has been traditionally considered a static terminal condition, it is now recognized as a dynamic stepwise process, which involves a plethora of factors that coordinately ensure its correct progress. We have identified a lncRNA that is specifically expressed at later stages of senescence induction to maintain the metabolic balance of these cells. Such precise induction is linked to timely transcriptional activation mediated by the SASP master regulator C/EBPβ, a transcription factor known to promote the later inflammatory phase of the senescent program.[31] Remarkably, depletion of *sin-lncRNA* is linked to the activation of some inflammatory signals as well as extracellular matrix remodeling pathways, gene networks that are induced during the second phase of senescence induction. *sin-lncRNA* depletion reinforces the senescence response, altering many of the canonical senescence markers. This is likely a consequence of the augmented ROS production, which feeds forward the senescent phenotype.

Mitochondria are the main source of ROS in the cell.[57] Interestingly, one of the most deregulated pathways upon *sin-lncRNA* depletion is OXPHOS, which reflects mitochondrial dysfunction and results in high levels of ROS production.[58] High levels of ROS are critical for the onset and maintenance of cellular senescence, although it remains difficult to decipher whether they are the cause or consequence of the senescence process.[59] Nevertheless, several factors are involved in feedback mechanisms to prevent an uncontrolled ROS increase.[60] We have found that *sin-lncRNA* interacts with DLST, an enzyme of the TCA cycle, a process that is tightly interconnected to OXPHOS and a main source of ROS.[61] Interestingly, it has been previously shown that the KGDH complex is sensitive to ROS and involved in ROS production,[62] and inhibition of this enzyme might be critical in the metabolic deficiency induced by oxidative stress.[63] DLST depletion in senescent cells mimics *sin-lncRNA* knockdown by exacerbating growth arrest and β-galactosidase staining. Moreover, both *sin-lncRNA* and DLST downregulation result in increased ECAR and lactate production, suggesting a shift in the energy production pathway toward glycolysis. This may reflect a mechanism for escaping the restrictions caused by the increased oxidative stress. Interestingly, we have observed different effects when measuring the specific glutamine-derived TCA metabolites by LC-MS. Whereas inhibition of DLST strongly affects different steps of the TCA cycle, sin-lncRNA depletion does not result in such changes. The fact that different enzymes involved in the GABA shunt pathway are found to be overexpressed in these cells would explain these differences as it could contribute to maintaining TCA cycle activity in *sin-lncRNA*-depleted cells. This compensatory mechanism might also explain the fact that the basal respiration rate is not affected in *sin-lncRNA* knockdown cells, while the maximal respiration and the spare capacity are strongly decreased. Previous studies have described similar changes in mitochondrial capacity following silencing of the AAC ADP/ATP carriers, suggesting an important role for AACs in maintaining metabolic spare capacity.[64] Besides, inhibition of ATP synthase activity has been shown to promote metabolic rewiring to an enhanced aerobic glycolysis and the subsequent production of mitochondrial ROS.[37] Additional transcriptional alterations observed in metabolic genes such as ADP/ATP carriers might contribute to the phenotypic alterations observed upon *sin-lncRNA* knockdown.

Of note, we have identified as a potential *sin-lncRNA* interactor DDX28, which plays a role in OXPHOS and is also known to shuttle from the nucleus to the cytoplasm and mitochondria.[47] Therefore, we cannot exclude that *sin-lncRNA* might regulate other aspects of metabolism at the interface between cytoplasm and mitochondria or even other subcellular compartments. Interestingly, TCA enzymes have been found to translocate into the nucleus where they have roles in epigenetic regulation.[65–68] In particular, the KGDH complex, which generates succinyl-CoA, has been demonstrated to contribute to histone succinylation affecting expression of cell cycle genes[52] and altering metabolic states.[69] Overexpression of wild-type DLST is able to reproduce the effect of *sin-lncRNA* depletion on the transcription of metabolic genes, whereas a mutant which is not able to translocate to the nucleus does not (Figure 5E). Although the mechanism underlying this response needs to be further explored, these results indicate that the two forms have a different impact in transcriptional regulation. Interestingly, we observed a significant overlap between the genes deregulated by the knockdown of *sin-lncRNA* and the H3K79Succ peaks, with key metabolic genes affected[52] (Figures S6D, S6E, and 5F), suggesting that *sin-lncRNA* knockdown leads to changes in this histone mark regulating metabolic transcription programs. Thus, while sin-lncRNA expression in senescent cells is relatively high (~80 molecules per cell), it does not appear sufficient to serve as a structural scaffold for the KGDH complex. Instead, sin-lncRNA likely functions as a signal amplifier, linking mitochondrial processes to nuclear transcriptional programs.

The molecular mechanism of interaction between DLST (KGDH complex) and sin-lncRNA and how it influences the localization of the protein remain to be understood; our observations are in line with the growing evidence that many metabolic enzymes interact with regulatory RNAs.[27,70] For instance, recent pre-print work from the Hentze laboratory has shown that RNA is required for proper mitochondrial import of ATP5A1.[71] All this emerging evidence suggests the presence of an undiscovered RNA-protein network with significant implications for regulating cellular energy metabolism.

Platinum-based therapies, currently used as the first line of treatment for patients with ovarian cancer, are known to induce senescence in cancer cells.[72] Although therapy-induced senescence has been considered a desirable outcome of cancer therapy, the activation of the senescence program has been shown to induce the rewiring of cellular metabolism, promoting the protumorigenic and pro-metastatic potential of ovarian cancer cells.[73] Here, we show that *sin-lncRNA* is specifically induced in ovarian cancer cells that undergo senescence and contributes to sustain the metabolic demands to maintain senescence in cancer cells upon drug treatment. Emerging studies link metabolic reprogramming to cancer drug resistance.[74] Indeed, cisplatin-resistant cells exhibit increased FA uptake,

accompanied by decreased glucose uptake and lipogenesis, indicating reprogramming from glucose to FA-dependent anabolic and energy metabolism.[75] Importantly, other metabolic processes affected by *sin-lncRNA* depletion in senescent fibroblasts seen at the transcriptional level include FA metabolism. Depletion of *sin-lncRNA* might sensitize ovarian tumor cells to cisplatin by metabolic reprogramming at different levels.

Metabolic enzymes required for the TCA cycle have been shown to affect senescence by regulating p53.[76] Importantly, advances in the field of RNA interactome capture have demonstrated that the interplay between metabolic enzymes and RNA is broader than previously considered.[27,70] These studies have revealed the RNA binding capacity of many enzymes, although the precise mechanism or the physiological relevance requires deeper characterization. Emerging evidence indicates that lncRNAs may contribute to cellular processes in order to adapt and coordinate mitochondrial function to adjust their activities to the environmental conditions.[27,77,78] We propose that distinct cellular states or stresses that result in metabolic changes involve the function of ncRNAs that contribute to the reconfiguration of the cell metabolism. The exquisite specificity of *sin-lncRNA* in senescence highlights its potential role as a therapeutic target. This discovery paves the way for better comprehension of therapy-induced senescence and its associated implications.

Limitations of the study

Here, we provide important insights into the role of *sin-lncRNA* in cellular senescence and its effects on metabolic reprogramming. However, several limitations should be considered. Our results suggest that high levels of ROS are causing an increased senescence phenotype, but it remains challenging to determine whether ROS are the cause or consequence of senescence. The feedback mechanisms involved in ROS regulation require more detailed investigation to clarify the causality. While we show that *sin-lncRNA* interacts with the metabolic enzyme DLST (KGDH complex), the molecular mechanism underlying this interaction remains unclear. Although *sin-lncRNA* is relatively abundant in senescent cells, it is unlikely that it involves a structural core component of the KGDH complex. Instead, our data suggest that it is functioning by amplifying signals and linking mitochondrial functions to nuclear transcriptional activities. Moreover, we also find an interaction with DDX28, a protein that regulates OXPHOS and also known to shuttle from the nucleus to the cytoplasm and mitochondria. Additional experiments are required to investigate whether *sin-lncRNA* might regulate other aspects of metabolisms by interacting with other proteins.

RESOURCE AVAILABILITY

Lead contact

Further information and requests for resources and reagents should be directed to and will be fulfilled by the lead contact, Dr. Maite Huarte (maitehuarte@unav.es).

Materials availability

Materials originated in the study can be requested through the lead contact.

Data and code availability

RNA-seq data from proliferating and senescent IMR90 fibroblasts were retrieved from public data (GEO: GSE61130).[28] RNA-seq data from replicative senescence mitoplasts were retrieved from public data (GEO: GSE73458).[46] H3K79Succ peaks were retrieved from public data (GEO: GSE97994).[52]

RNA-seq data of *sin-lncRNA* knockdown and control senescent cells have been deposited in NCBI's Gene Expression Omnibus (GEO) and are accessible through GEO[79] repository under the accession number GEO: GSE241620. The mass spectrometry data have been deposited to the ProteomeXchange Consortium via the PRIDE[80] partner repository with the dataset identifier PRIDE: PXD044718. Metabolomic data are available at the NIH Common Fund's National Metabolomics Data Repository, Metabolomics Workbench[81] with the ID Metabolomics Workbench: ST003869. Accession numbers are listed in the key resources table.

ACKNOWLEDGMENTS

We thank Eva Santamaría for her input and help with the Seahorse experiments. We thank Beatriz Tavira (CIMA, Universidad de Navarra) for providing the COD362 cells. We thank Sebastiaan Martijn Van Liempd and Juan Manuel Falcón (Metabolomic Platform, CIC bioGUNE) and Lorea Válcarcel (UPV) and Arkaitz Carracerdo (CIC bioGUNE) for their input on the metabolic experiments. We thank Lukas Bethlehem for helping interpreting the metabolomic data. We thank Victor Segura and Eli Guruceaga for the guilt-by-association analysis. We thank Jesus Gil (MRC, London) for his input. We acknowledge the ENCODE project and The Cancer Genome Atlas database for their valuable datasets. We thank the rest of the Huarte lab for contributing with helpful discussions. The work was supported by Project PID2023-147980NB-100 financed by MICIU/AEI/10.13039/501100011033 and FEDER, UE , 'La Caixa' Foundation (LCF/PR/HR21/00176), Worldwide Cancer Research grant 25-0335, and Ayuda Proyectos Generales AECC 2024. M.M. was funded by an MSCA fellowship (HORIZON-MSCA- 2021-PF-01: 101066499) and currently by Ministerio de Ciencia e Innovación through Programa Ramón y Cajal (RYC2022-036819-I) . L.P.-C. is supported by Instituto de Salud Carlos III (Ministerio de Ciencia e Innovación) through a Miguel Servet contract (CP22/00005), co-funded by the European Union.

AUTHOR CONTRIBUTIONS

M.H., M.M., and E. Grossi. conceived the study. E. Grossi., M.M., and M.H. designed the experiments, analyzed the data, and wrote the manuscript with the comments of co-authors. E. Grossi., F.P.M., J.G., and M.M. performed the experiments. E. Goñi., J.M.F.-J., and A.A. performed bioinformatic analyses. L.P.-C. provided interpretation and developed figures of the metabolomics experiment. N.H. contributed to the original setup of the project.

DECLARATION OF INTERESTS

The authors declare no competing interests.

STAR★METHODS

Detailed methods are provided in the online version of this paper and include the following:

- KEY RESOURCES TABLE
- EXPERIMENTAL MODEL AND STUDY PARTICIPANT DETAILS
  - Cells
- METHOD DETAILS
  - Senescence induction and cell treatments
  - Irradiation
  - RNAi studies
  - CRISPR-Cas9 gene editing
  - Cell proliferation assays
  - Apoptosis staining
  - SA-β-gal staining

- ROS/RNS measurement assay
- Oxygen consumption rate and extracellular acidification
- Lactate measurements
- Liquid chromatographic -mass spectrometry (LC-MS) metabolomics
- Sample preparation and LC/MS methods
- Immunofluorescence and RNA fluorescence *in situ* hybridization (RNA-FISH)
- Protein extraction and immunoblot analysis
- Cellular fractionation
- Mitochondria isolation
- Native RNA immunoprecipitation
- *In vitro* RNA pulldown
- Chromatin immunoprecipitation (ChIP)
- RNA extraction and RT-qPCR analysis
- RNA sequencing and data analysis
- *Sin-lncRNA* expression analysis in tumor samples

- QUANTIFICATION AND STATISTICAL ANALYSIS

SUPPLEMENTAL INFORMATION

Supplemental information can be found online at https://doi.org/10.1016/j.celrep.2025.115747.

Received: August 24, 2023
Revised: March 21, 2025
Accepted: May 6, 2025
Published: May 21, 2025

REFERENCES

1. Kuilman, T., Michaloglou, C., Mooi, W.J., and Peeper, D.S. (2010). The essence of senescence. Genes Dev. *24*, 2463–2479. https://doi.org/10.1101/gad.1971610.
2. Kuilman, T., Michaloglou, C., Vredeveld, L.C.W., Douma, S., van Doorn, R., Desmet, C.J., Aarden, L.A., Mooi, W.J., and Peeper, D.S. (2008). Oncogene-induced senescence relayed by an interleukin-dependent inflammatory network. Cell *133*, 1019–1031. https://doi.org/10.1016/j.cell.2008.03.039.
3. Acosta, J.C., O'Loghlen, A., Banito, A., Guijarro, M.V., Augert, A., Raguz, S., Fumagalli, M., Da Costa, M., Brown, C., Popov, N., et al. (2008). Chemokine signaling via the CXCR2 receptor reinforces senescence. Cell *133*, 1006–1018. https://doi.org/10.1016/j.cell.2008.03.038.
4. Coppé, J.P.,, Patil, C.K., Rodier, F., Sun, Y., Muñoz, D.P., Goldstein, J., Nelson, P.S., Desprez, P.-Y., and Campisi, J. (2008). Senescence-associated secretory phenotypes reveal cell-nonautonomous functions of oncogenic RAS and the p53 tumor suppressor. PLoS Biol. *6*, 2853–2868. https://doi.org/10.1371/journal.pbio.0060301.
5. Coppé, J.P., Desprez, P.Y., Krtolica, A., and Campisi, J. (2010). The senescence-associated secretory phenotype: the dark side of tumor suppression. Annu. Rev. Pathol. *5*, 99–118. https://doi.org/10.1146/annurev-pathol-121808-102144.
6. Nardella, C., Clohessy, J.G., Alimonti, A., and Pandolfi, P.P. (2011). Pro-senescence therapy for cancer treatment. Nat. Rev. Cancer *11*, 503–511. https://doi.org/10.1038/nrc3057.
7. Milanovic, M., Fan, D.N.Y., Belenki, D., Däbritz, J.H.M., Zhao, Z., Yu, Y., Dörr, J.R., Dimitrova, L., Lenze, D., Monteiro Barbosa, I.A., et al. (2018). Senescence-associated reprogramming promotes cancer stemness. Nature *553*, 96–100. https://doi.org/10.1038/nature25167.
8. Dorr, J.R., Yu, Y., Milanovic, M., Beuster, G., Zasada, C., Däbritz, J.H.M., Lisec, J., Lenze, D., Gerhardt, A., Schleicher, K., et al. (2013). Synthetic lethal metabolic targeting of cellular senescence in cancer therapy. Nature *501*, 421–425. https://doi.org/10.1038/nature12437.
9. Gonzalez-Gualda, E., Baker, A.G., Fruk, L., and Munoz-Espin, D. (2021). A guide to assessing cellular senescence in vitro and in vivo. FEBS J. *288*, 56–80. https://doi.org/10.1111/febs.15570.
10. Kwon, S.M., Hong, S.M., Lee, Y.K., Min, S., and Yoon, G. (2019). Metabolic features and regulation in cell senescence. BMB Rep. *52*, 5–12. https://doi.org/10.5483/BMBRep.2019.52.1.291.
11. Lee, A.C., Fenster, B.E., Ito, H., Takeda, K., Bae, N.S., Hirai, T., Yu, Z.X., Ferrans, V.J., Howard, B.H., and Finkel, T. (1999). Ras proteins induce senescence by altering the intracellular levels of reactive oxygen species. J. Biol. Chem. *274*, 7936–7940. https://doi.org/10.1074/jbc.274.12.7936.
12. Moiseeva, O., Bourdeau, V., Roux, A., Deschênes-Simard, X., and Ferbeyre, G. (2009). Mitochondrial dysfunction contributes to oncogene-induced senescence. Mol. Cell Biol. *29*, 4495–4507. https://doi.org/10.1128/MCB.01868-08.
13. Mattick, J.S., Amaral, P.P., Carninci, P., Carpenter, S., Chang, H.Y., Chen, L.L., Chen, R., Dean, C., Dinger, M.E., Fitzgerald, K.A., et al. (2023). Long non-coding RNAs: definitions, functions, challenges and recommendations. Nat. Rev. Mol. Cell Biol. *24*, 430–447. https://doi.org/10.1038/s41580-022-00566-8.
14. Statello, L., Guo, C.J., Chen, L.L., and Huarte, M. (2021). Gene regulation by long non-coding RNAs and its biological functions. Nat. Rev. Mol. Cell Biol. *22*, 96–118. https://doi.org/10.1038/s41580-020-00315-9.
15. Qureshi, I.A., and Mehler, M.F. (2012). Emerging roles of non-coding RNAs in brain evolution, development, plasticity and disease. Nat. Rev. Neurosci. *13*, 528–541. https://doi.org/10.1038/nrn3234.
16. Huarte, M. (2015). The emerging role of lncRNAs in cancer. Nat. Med. *21*, 1253–1261. https://doi.org/10.1038/nm.3981.
17. Abdelmohsen, K., Panda, A., Kang, M.J., Xu, J., Selimyan, R., Yoon, J.H., Martindale, J.L., De, S., Wood, W.H., 3rd, Becker, K.G., and Gorospe, M. (2013). Senescence-associated lncRNAs: senescence-associated long noncoding RNAs. Aging Cell *12*, 890–900. https://doi.org/10.1111/acel.12115.
18. Montes, M., Nielsen, M.M., Maglieri, G., Jacobsen, A., Højfeldt, J., Agrawal-Singh, S., Hansen, K., Helin, K., van de Werken, H.J.G., Pedersen, J.S., and Lund, A.H. (2015). The lncRNA MIR31HG regulates p16 (INK4A) expression to modulate senescence. Nat. Commun. *6*, 6967. https://doi.org/10.1038/ncomms7967.
19. Montes, M., Lubas, M., Arendrup, F.S., Mentz, B., Rohatgi, N., Tumas, S., Harder, L.M., Skanderup, A.J., Andersen, J.S., and Lund, A.H. (2021). The long non-coding RNA MIR31HG regulates the senescence associated secretory phenotype. Nat. Commun. *12*, 2459. https://doi.org/10.1038/s41467-021-22746-4.
20. Montes, M., and Lund, A.H. (2016). Emerging roles of lncRNAs in senescence. FEBS J. *283*, 2414–2426. https://doi.org/10.1111/febs.13679.
21. Puvvula, P.K., Desetty, R.D., Pineau, P., Marchio, A., Moon, A., Dejean, A., and Bischof, O. (2014). Long noncoding RNA PANDA and scaffold-attachment-factor SAFA control senescence entry and exit. Nat. Commun. *5*, 5323. https://doi.org/10.1038/ncomms6323.
22. Grossi, E., Raimondi, I., Goñi, E., González, J., Marchese, F.P., Chapaprieta, V., Martín-Subero, J.I., Guo, S., and Huarte, M. (2020). A lncRNA-SWI/SNF complex crosstalk controls transcriptional activation at specific promoter regions. Nat. Commun. *11*, 936. https://doi.org/10.1038/s41467-020-14623-3.
23. Zhu, Y., Jin, L., Shi, R., Li, J., Wang, Y., Zhang, L., Liang, C.Z., Narayana, V. K., De Souza, D.P., Thorne, R.F., et al. (2022). The long noncoding RNA glycoLINC assembles a lower glycolytic metabolon to promote glycolysis. Mol. Cell *82*, 542–554.e6. https://doi.org/10.1016/j.molcel.
24. Wang, P., Xu, J., Wang, Y., and Cao, X. (2017). An interferon-independent lncRNA promotes viral replication by modulating cellular metabolism. Science *358*, 1051–1055. https://doi.org/10.1126/science.aao0409.
25. Gandhi, M., Groß, M., Holler, J.M., Coggins, S.A., Patil, N., Leupold, J.H., Munschauer, M., Schenone, M., Hartigan, C.R., Allgayer, H., et al. (2020). The lncRNA lincNMR regulates nucleotide metabolism via a YBX1 - RRM2

axis in cancer. Nat. Commun. *11*, 3214. https://doi.org/10.1038/s41467-020-17007-9.

26. Ding, C., Yu, Z., Sefik, E., Zhou, J., Kaffe, E., Wang, G., Li, B., Flavell, R.A., Hu, W., Ye, Y., and Li, H.B. (2023). A T(reg)-specific long noncoding RNA maintains immune-metabolic homeostasis in aging liver. Nat. Aging *3*, 813–828. https://doi.org/10.1038/s43587-023-00428-8.
27. Castello, A., Hentze, M.W., and Preiss, T. (2015). Metabolic Enzymes Enjoying New Partnerships as RNA-Binding Proteins. Trends Endocrinol. Metabol. *26*, 746–757. https://doi.org/10.1016/j.tem.2015.09.012.
28. Herranz, N., Gallage, S., Mellone, M., Wuestefeld, T., Klotz, S., Hanley, C. J., Raguz, S., Acosta, J.C., Innes, A.J., Banito, A., et al. (2015). mTOR regulates MAPKAPK2 translation to control the senescence-associated secretory phenotype. Nat. Cell Biol. *17*, 1205–1217. https://doi.org/10.1038/ncb3225.
29. Vater, C.A., Bartle, L.M., Dionne, C.A., Littlewood, T.D., and Goldmacher, V.S. (1996). Induction of apoptosis by tamoxifen-activation of a p53-estrogen receptor fusion protein expressed in E1A and T24 H-ras transformed p53-/- mouse embryo fibroblasts. Oncogene *13*, 739–748.
30. ENCODE Project Consortium (2012). An integrated encyclopedia of DNA elements in the human genome. Nature *489*, 57–74. https://doi.org/10.1038/nature11247.
31. Hoare, M., Ito, Y., Kang, T.W., Weekes, M.P., Matheson, N.J., Patten, D.A., Shetty, S., Parry, A.J., Menon, S., Salama, R., et al. (2016). NOTCH1 mediates a switch between two distinct secretomes during senescence. Nat. Cell Biol. *18*, 979–992. https://doi.org/10.1038/ncb3397.
32. Innes, A.J., and Gil, J. (2019). IMR90 ER:RAS: A Cell Model of Oncogene-Induced Senescence. Methods Mol. Biol. *1896*, 83–92. https://doi.org/10.1007/978-1-4939-8931-7_9.
33. Woods, D., Parry, D., Cherwinski, H., Bosch, E., Lees, E., and McMahon, M. (1997). Raf-induced proliferation or cell cycle arrest is determined by the level of Raf activity with arrest mediated by p21Cip1. Mol. Cell Biol. *17*, 5598–5611. https://doi.org/10.1128/MCB.17.9.5598.
34. Nuskova, H., Mráček, T., Mikulová, T., Vrbacký, M., Kovářová, N., Kovalčíková, J., Pecina, P., and Houštěk, J. (2015). Mitochondrial ATP synthasome: Expression and structural interaction of its components. Biochem. Biophys. Res. Commun. *464*, 787–793. https://doi.org/10.1016/j.bbrc.2015.07.034.
35. Hutter, E., Renner, K., Pfister, G., Stöckl, P., Jansen-Dürr, P., and Gnaiger, E. (2004). Senescence-associated changes in respiration and oxidative phosphorylation in primary human fibroblasts. Biochem. J. *380*, 919–928. https://doi.org/10.1042/BJ20040095.
36. Zhang, J., and Zhang, Q. (2019). Using Seahorse Machine to Measure OCR and ECAR in Cancer Cells. Methods Mol. Biol. *1928*, 353–363. https://doi.org/10.1007/978-1-4939-9027-6_18.
37. Martinez-Reyes, I., and Cuezva, J.M. (2014). The H(+)-ATP synthase: a gate to ROS-mediated cell death or cell survival. Biochim. Biophys. Acta *1837*, 1099–1112. https://doi.org/10.1016/j.bbabio.2014.03.010.
38. Santamaria, G., Martinez-Diez, M., Fabregat, I., and Cuezva, J.M. (2006). Efficient execution of cell death in non-glycolytic cells requires the generation of ROS controlled by the activity of mitochondrial H+-ATP synthase. Carcinogenesis *27*, 925–935. https://doi.org/10.1093/carcin/bgi315.
39. Ni, R., Zheng, D., Xiong, S., Hill, D.J., Sun, T., Gardiner, R.B., Fan, G.C., Lu, Y., Abel, E.D., Greer, P.A., and Peng, T. (2016). Mitochondrial Calpain-1 Disrupts ATP Synthase and Induces Superoxide Generation in Type 1 Diabetic Hearts: A Novel Mechanism Contributing to Diabetic Cardiomyopathy. Diabetes *65*, 255–268. https://doi.org/10.2337/db15-0963.
40. Johnson, K.M., Chen, X., Boitano, A., Swenson, L., Opipari, A.W., Jr., and Glick, G.D. (2005). Identification and validation of the mitochondrial F1F0-ATPase as the molecular target of the immunomodulatory benzodiazepine Bz-423. Chem. Biol. *12*, 485–496. https://doi.org/10.1016/j.chembiol.2005.02.012.
41. Vizioli, M.G., Liu, T., Miller, K.N., Robertson, N.A., Gilroy, K., Lagnado, A. B., Perez-Garcia, A., Kiourtis, C., Dasgupta, N., Lei, X., et al. (2020). Mitochondria-to-nucleus retrograde signaling drives formation of cytoplasmic chromatin and inflammation in senescence. Genes Dev. *34*, 428–445. https://doi.org/10.1101/gad.331272.119.
42. Velarde, M.C., Flynn, J.M., Day, N.U., Melov, S., and Campisi, J. (2012). Mitochondrial oxidative stress caused by Sod2 deficiency promotes cellular senescence and aging phenotypes in the skin. Aging (Albany NY) *4*, 3–12. https://doi.org/10.18632/aging.100423.
43. Macip, S., Igarashi, M., Fang, L., Chen, A., Pan, Z.Q., Lee, S.W., and Aaronson, S.A. (2002). Inhibition of p21-mediated ROS accumulation can rescue p21-induced senescence. EMBO J. *21*, 2180–2188. https://doi.org/10.1093/emboj/21.9.2180.
44. Staal, F.J., Roederer, M., Herzenberg, L.A., and Herzenberg, L.A. (1990). Intracellular thiols regulate activation of nuclear factor kappa B and transcription of human immunodeficiency virus. Proc. Natl. Acad. Sci. USA *87*, 9943–9947. https://doi.org/10.1073/pnas.87.24.9943.
45. Leucci, E., Vendramin, R., Spinazzi, M., Laurette, P., Fiers, M., Wouters, J., Radaelli, E., Eyckerman, S., Leonelli, C., Vanderheyden, K., et al. (2016). Melanoma addiction to the long non-coding RNA SAMMSON. Nature *531*, 518–522. https://doi.org/10.1038/nature17161.
46. Noh, J.H., Kim, K.M., Abdelmohsen, K., Yoon, J.H., Panda, A.C., Munk, R., Kim, J., Curtis, J., Moad, C.A., Wohler, C.M., et al. (2016). HuR and GRSF1 modulate the nuclear export and mitochondrial localization of the lncRNA RMRP. Genes Dev. *30*, 1224–1239. https://doi.org/10.1101/gad.276022.115.
47. Tu, Y.T., and Barrientos, A. (2015). The Human Mitochondrial DEAD-Box Protein DDX28 Resides in RNA Granules and Functions in Mitoribosome Assembly. Cell Rep. *10*, 854–864. https://doi.org/10.1016/j.celrep.2015.01.033.
48. Sheu, K.F., and Blass, J.P. (1999). The alpha-ketoglutarate dehydrogenase complex. Ann. N. Y. Acad. Sci. *893*, 61–78. https://doi.org/10.1111/j.1749-6632.1999.tb07818.x.
49. Street, L.A., Rothamel, K.L., Brannan, K.W., Jin, W., Bokor, B.J., Dong, K., Rhine, K., Madrigal, A., Al-Azzam, N., Kim, J.K., et al. (2024). Large-scale map of RNA-binding protein interactomes across the mRNA life cycle. Mol. Cell *84*, 3790–3809.e8. https://doi.org/10.1016/j.molcel.2024.08.030.
50. Shen, N., Korm, S., Karantanos, T., Li, D., Zhang, X., Ritou, E., Xu, H., Lam, A., English, J., Zong, W.X., et al. (2021). DLST-dependence dictates metabolic heterogeneity in TCA-cycle usage among triple-negative breast cancer. Commun. Biol. *4*, 1289. https://doi.org/10.1038/s42003-021-02805-8.
51. Qattan, A.T., Radulovic, M., Crawford, M., and Godovac-Zimmermann, J. (2012). Spatial distribution of cellular function: the partitioning of proteins between mitochondria and the nucleus in MCF7 breast cancer cells. J. Proteome Res. *11*, 6080–6101. https://doi.org/10.1021/pr300736v.
52. Wang, Y., Guo, Y.R., Liu, K., Yin, Z., Liu, R., Xia, Y., Tan, L., Yang, P., Lee, J.H., Li, X.J., et al. (2017). KAT2A coupled with the alpha-KGDH complex acts as a histone H3 succinyltransferase. Nature *552*, 273–277. https://doi.org/10.1038/nature25003.
53. Gibson, G.E., Blass, J.P., Beal, M.F., and Bunik, V. (2005). V. The alpha-ketoglutarate–dehydrogenase complex: a mediator between mitochondria and oxidative stress in neurodegeneration. Mol. Neurobiol. *31*, 43–63. https://doi.org/10.1385/mn:31:1-3:043.
54. Bodineau, C., Tomé, M., Courtois, S., Costa, A.S.H., Sciacovelli, M., Rousseau, B., Richard, E., Vacher, P., Parejo-Pérez, C., Bessede, E., et al. (2021). Two parallel pathways connect glutamine metabolism and mTORC1 activity to regulate glutamoptosis. Nat. Commun. *12*, 4814. https://doi.org/10.1038/s41467-021-25079-4.
55. Frigola, J., Remus, D., Mehanna, A., and Diffley, J.F.X. (2013). ATPase-dependent quality control of DNA replication origin licensing. Nature *495*, 339–343. https://doi.org/10.1038/nature11920.

56. Alvarez-Abril, B., Garcia-Martinez, E., and Galluzzi, L. (2022). Platinum-based chemotherapy inflames the ovarian carcinoma microenvironment through cellular senescence. OncoImmunology *11*, 2052411. https://doi.org/10.1080/2162402X.2022.2052411.

57. Murphy, M.P. (2009). How mitochondria produce reactive oxygen species. Biochem. J. *417*, 1–13. https://doi.org/10.1042/BJ20081386.

58. Hamanaka, R.B., and Chandel, N.S. (2010). Mitochondrial reactive oxygen species regulate cellular signaling and dictate biological outcomes. Trends Biochem. Sci. *35*, 505–513. https://doi.org/10.1016/j.tibs.2010.04.002.

59. Davalli, P., Mitic, T., Caporali, A., Lauriola, A., D'Arca, D., and ROS, D. (2016). Cell Senescence, and Novel Molecular Mechanisms in Aging and Age-Related Diseases. Oxid. Med. Cell. Longev. *2016*, 3565127. https://doi.org/10.1155/2016/3565127.

60. Wei, Z., Guo, H., Liu, Z., Zhang, X., Liu, Q., Qian, Y., Gong, Y., and Shao, C. (2015). CUL4B impedes stress-induced cellular senescence by dampening a p53-reactive oxygen species positive feedback loop. Free Radic. Biol. Med. *79*, 1–13. https://doi.org/10.1016/j.freeradbiomed.2014.11.010.

61. Martinez-Reyes, I., and Chandel, N.S. (2020). Mitochondrial TCA cycle metabolites control physiology and disease. Nat. Commun. *11*, 102. https://doi.org/10.1038/s41467-019-13668-3.

62. Hansen, G.E., and Gibson, G.E. (2022). The alpha-Ketoglutarate Dehydrogenase Complex as a Hub of Plasticity in Neurodegeneration and Regeneration. Int. J. Mol. Sci. *23*, 12403. https://doi.org/10.3390/ijms232012403.

63. Tretter, L., and Adam-Vizi, V. (2000). Inhibition of Krebs cycle enzymes by hydrogen peroxide: A key role of [alpha]-ketoglutarate dehydrogenase in limiting NADH production under oxidative stress. J. Neurosci. *20*, 8972–8979. https://doi.org/10.1523/JNEUROSCI.20-24-08972.2000.

64. Hoogstraten, C.A., Jacobs, M.M.E., de Boer, G., van de Wal, M.A.E., Koopman, W.J.H., Smeitink, J.A.M., Russel, F.G.M., and Schirris, T.J.J. (2023). Metabolic impact of genetic and chemical ADP/ATP carrier inhibition in renal proximal tubule epithelial cells. Arch. Toxicol. *97*, 1927–1941. https://doi.org/10.1007/s00204-023-03510-7.

65. Sutendra, G., Kinnaird, A., Dromparis, P., Paulin, R., Stenson, T.H., Haromy, A., Hashimoto, K., Zhang, N., Flaim, E., and Michelakis, E.D. (2014). A nuclear pyruvate dehydrogenase complex is important for the generation of acetyl-CoA and histone acetylation. Cell *158*, 84–97. https://doi.org/10.1016/j.cell.2014.04.046.

66. Kafkia, E., Andres-Pons, A., Ganter, K., Seiler, M., Smith, T.S., Andrejeva, A., Jouhten, P., Pereira, F., Franco, C., Kuroshchenkova, A., et al. (2022). Operation of a TCA cycle subnetwork in the mammalian nucleus. Sci. Adv. *8*, eabq5206. https://doi.org/10.1126/sciadv.abq5206.

67. Li, W., Long, Q., Wu, H., Zhou, Y., Duan, L., Yuan, H., Ding, Y., Huang, Y., Wu, Y., Huang, J., et al. (2022). Nuclear localization of mitochondrial TCA cycle enzymes modulates pluripotency via histone acetylation. Nat. Commun. *13*, 7414. https://doi.org/10.1038/s41467-022-35199-0.

68. Chen, J., Guccini, I., Di Mitri, D., Brina, D., Revandkar, A., Sarti, M., Pasquini, E., Alajati, A., Pinton, S., Losa, M., et al. (2018). Compartmentalized activities of the pyruvate dehydrogenase complex sustain lipogenesis in prostate cancer. Nat. Genet. *50*, 219–228. https://doi.org/10.1038/s41588-017-0026-3.

69. Mellid, S., García, F., Leandro-García, L.J., Díaz-Talavera, A., Martínez-Montes, Á.M., Gil, E., Calsina, B., Monteagudo, M., Letón, R., Roldán-Romero, J.M., et al. (2023). DLST mutations in pheochromocytoma and paraganglioma cause proteome hyposuccinylation and metabolic remodeling. Cancer Commun. *43*, 838–843. https://doi.org/10.1002/cac2.12427.

70. Castello, A., Horos, R., Strein, C., Fischer, B., Eichelbaum, K., Steinmetz, L.M., Krijgsveld, J., and Hentze, M.W. (2016). Comprehensive Identification of RNA-Binding Proteins by RNA Interactome Capture. Methods Mol. Biol. *1358*, 131–139. https://doi.org/10.1007/978-1-4939-3067-8_8.

71. Chatterjee, A., Noble, M., Sekaran, T., Ravi, V., Ferring–Appel, D., Schwarzl, T., Rampelt, H., and Hentze, M.W. (2024). RNA promotes mitochondrial import of F1-ATP synthase subunit alpha (ATP5A1). Preprint at bioRxiv. https://doi.org/10.1101/2024.08.19.608659.

72. Ewald, J.A., Desotelle, J.A., Wilding, G., and Jarrard, D.F. (2010). Therapy-induced senescence in cancer. J. Natl. Cancer Inst. *102*, 1536–1546. https://doi.org/10.1093/jnci/djq364.

73. Pardella, E., Pranzini, E., Nesi, I., Parri, M., Spatafora, P., Torre, E., Muccilli, A., Castiglione, F., Fambrini, M., Sorbi, F., et al. (2022). Therapy-Induced Stromal Senescence Promoting Aggressiveness of Prostate and Ovarian Cancer. Cells *11*, 4026. https://doi.org/10.3390/cells11244026.

74. Pranzini, E., Pardella, E., Paoli, P., Fendt, S.M., and Taddei, M.L. (2021). Metabolic Reprogramming in Anticancer Drug Resistance: A Focus on Amino Acids. Trends Cancer *7*, 682–699. https://doi.org/10.1016/j.trecan.2021.02.004.

75. Tan, Y., Li, J., Zhao, G., Huang, K.C., Cardenas, H., Wang, Y., Matei, D., and Cheng, J.X. (2022). Metabolic reprogramming from glycolysis to fatty acid uptake and beta-oxidation in platinum-resistant cancer cells. Nat. Commun. *13*, 4554. https://doi.org/10.1038/s41467-022-32101-w.

76. Jiang, P., Du, W., Mancuso, A., Wellen, K.E., and Yang, X. (2013). Reciprocal regulation of p53 and malic enzymes modulates metabolism and senescence. Nature *493*, 689–693. https://doi.org/10.1038/nature11776.

77. Zhang, H., Xu, R., Li, B., Xin, Z., Ling, Z., Zhu, W., Li, X., Zhang, P., Fu, Y., Chen, J., et al. (2022). LncRNA NEAT1 controls the lineage fates of BMSCs during skeletal aging by impairing mitochondrial function and pluripotency maintenance. Cell Death Differ. *29*, 351–365. https://doi.org/10.1038/s41418-021-00858-0.

78. Vendramin, R., Marine, J.C., and Leucci, E. (2017). Non-coding RNAs: the dark side of nuclear-mitochondrial communication. EMBO J. *36*, 1123–1133. https://doi.org/10.15252/embj.201695546.

79. Edgar, R., Domrachev, M., and Lash, A.E. (2002). Gene Expression Omnibus: NCBI gene expression and hybridization array data repository. Nucleic Acids Res. *30*, 207–210. https://doi.org/10.1093/nar/30.1.207.

80. Perez-Riverol, Y., Bai, J., Bandla, C., García-Seisdedos, D., Hewapathirana, S., Kamatchinathan, S., Kundu, D.J., Prakash, A., Frericks-Zipper, A., Eisenacher, M., et al. (2022). The PRIDE database resources in 2022: a hub for mass spectrometry-based proteomics evidences. Nucleic Acids Res. *50*, D543–D552. https://doi.org/10.1093/nar/gkab1038.

81. Sud, M., Fahy, E., Cotter, D., Azam, K., Vadivelu, I., Burant, C., Edison, A., Fiehn, O., Higashi, R., Nair, K.S., et al. (2016). Metabolomics Workbench: An international repository for metabolomics data and metadata, metabolite standards, protocols, tutorials and training, and analysis tools. Nucleic Acids Res *44*, D463–D470. https://doi.org/10.1093/nar/gkv1042.

82. Dieterle, F., Ross, A., Schlotterbeck, G., and Senn, H. (2006). Probabilistic quotient normalization as robust method to account for dilution of complex biological mixtures. Application in 1H NMR metabonomics. Anal. Chem. *78*, 4281–4290. https://doi.org/10.1021/ac051632c.

83. Veselkov, K.A., Vingara, L.K., Masson, P., Robinette, S.L., Want, E., Li, J.V., Barton, R.H., Boursier-Neyret, C., Walther, B., Ebbels, T.M., et al. (2011). Optimized preprocessing of ultra-performance liquid chromatography/mass spectrometry urinary metabolic profiles for improved information recovery. Anal. Chem. *83*, 5864–5872. https://doi.org/10.1021/ac201065j.

84. Marin-Bejar, O., Mas, A.M., González, J., Martinez, D., Athie, A., Morales, X., Galduroz, M., Raimondi, I., Grossi, E., Guo, S., et al. (2017). The human lncRNA LINC-PINT inhibits tumor cell invasion through a highly conserved

sequence element. Genome Biol. *18*, 202. https://doi.org/10.1186/s13059-017-1331-y.

85. Liao, Y., Smyth, G.K., and Shi, W. (2014). featureCounts: an efficient general purpose program for assigning sequence reads to genomic features. Bioinformatics *30*, 923–930. https://doi.org/10.1093/bioinformatics/btt656.

86. Langmead, B., and Salzberg, S.L. (2012). Fast gapped-read alignment with Bowtie 2. Nat. Methods *9*, 357–359. https://doi.org/10.1038/nmeth.1923.

87. Liberzon, A., Birger, C., Thorvaldsdóttir, H., Ghandi, M., Mesirov, J.P., and Tamayo, P. (2015). The Molecular Signatures Database (MSigDB) hallmark gene set collection. Cell Syst. *1*, 417–425. https://doi.org/10.1016/j.cels.2015.12.004.

STAR★METHODS

KEY RESOURCES TABLE

REAGENT or RESOURCE	SOURCE	IDENTIFIER
Antibodies		
HRP-conjugated GAPDH (14C10)	CST	3683; RRID:AB_1642205
p53 (DO-1)	Santa Cruz	sc-126; RRID: AB_628082
p21 (F-5)	Santa Cruz	sc-6246; RRID:AB_628073
p16	BD Pharmingen	554079
C/EBP β (C-19)	Santa Cruz	sc-150; RRID:AB_2260363
Phospho-p53 [Ser15]	CST	9284; RRID:AB_331464
DLST	Sigma	HPA003-010; RRID:AB_1078679
DLST	Bethyl	A304-309A-T
H3	Abcam	ab10799; RRID:AB_470239
HRP-conjugated mouse IgG	CST	7076S; RRID:AB_330924
HRP-conjugated rabbit IgG	CST	7074S; RRID:AB_2099233
yH2A.X [Ser139]	Millipore	05–636; RRID:AB_309864
H3K9me3	Millipore	307–523
Alexa Fluor 488-conjugated mouse IgG	Thermo Fisher	a21202; RRID:AB_141607
Alexa Fluor 555-conjugated rabbit IgG	Thermo Fisher	a31572; RRID:AB_162543
Normal Rabbit IgG	CST	2729S; RRID:AB_1031062
Succinyl-Histone H3 (Lys79) Polyclonal Antibody	Life technologies	PA5-116784; RRID:AB_2901415
Chemicals, peptides, and recombinant proteins		
DMEM	GIBCO	41966029
FBS, fetal bovine serum	GIBCO	A5256801
Tetracycline-free tested serum	Clontech	A4736401
penicillin/streptomycin	Lonza	31985047
TRYPSIN-EDTA (1X) IN HBSS	GIBCO	25200056
T3 polymerase	Thermo-Scientific	EP0101
T7 polymerase	Thermo-Scientific	EP0112
opti-MEM	GIBCO	31985047
Lipofectamine 2000	Invitrogen	11668019
Polybrene	Santacruz	sc-134220
Neomycin	SIGMA	4727878001
Puromycin	SIGMA	P4512-1MLX10
Doxycicline	SIGMA	D5207-1G
N-Acetyl-L-cysteine	SIGMA	A9165
4-Hydroxitamoxifen	sigma	H6278
Crystal violet	Sigma	C0775
4 mM L-$^{13}C_5$-Glutamine	Cambridge Isotopes Laboratories	CLM-1822-H-0.1
methanol-free formaldehyde solution	Thermo Fisher	28908
Triethanolamine	Sigma	90279-100ML
Acetic Anhydride	Sigma	539996
Dextran sulfate	Sigma	D6001-50G
Formamide	Thermo Fisher	AM9342
αFAM-POD	Roche	11426346910
Saline sodium citrate 20x SSC	Sigma	S6639
Blocking Reagent	[Roche]	11096176001

(*Continued on next page*)

Continued

REAGENT or RESOURCE	SOURCE	IDENTIFIER
DAPI mounting solution	Thermo Fisher	P36931
cOmplete Protease Inhibitor Cocktail	Roche	5056489001
PhosSTOP phosphatase inhibitor	Roche	4906837001
MitoTracker Green	Thermo-Fisher	M7514
RNAsin	Promega	N2111
Dynabeads Protein A	Invitrogen	10002D
Dynabeads Protein G beads	Invitrogen	10004D
Dynabeads MyOne Streptavidin T1 beads	Invitrogen	2650042
G-50 MicroSpin columns	GE Healthcare	27533001
Proteinase K	NEB	P8107S
iTaq Universal SYBR Green supermix	Bio-Rad	1725124
DNase I	Invitrogen	18068015
TRI reagent	Sigma	T3809
Critical commercial assays		
Senescence β-Galactosidase Staining Kit	CST	9860
Pierce™ BCA Protein Assay Kits (100 mL)	Thermo Fisher	23227
MycoAlert Mycoplasma Detection Kit	Lonza	LT07-418
PE Annexin V Apoptosis Detection Kit I	BD Pharmingen	559763
OxiSelect *in vitro* ROS/RNS Assay Kit	Cell Biolabs	STA-347
LACT2 kit	Roche Diagnostics GmbH	766062
In-Fusion HD Cloning kit	Takara	639650
Seahorse XF Cell Mito Stress Test	Agilent	103015–100
TSA-Cy3	Perkin Elmer	NEL744B001KT
BrdU flow kit	BD Pharmingen	51-9000019AK
High-Capacity cDNA Reverse Transcription Kit	Applied Biosystem	4868813
SilverQuest Silver Staining Kit	Thermo Fisher	45–1001
QuickExtract DNA extraction solution	Lucigen	LGCQE09050
Deposited data		
RNA-seq of *sin-lncRNA* KD and control senescent cells	Gene Expression Omnibus (GEO)	GEO: GSE241620
Mass spectrometry *in vitro* pulldown	ProteomeXchange	PXD044718
Metabolomics	Metabolomics Workbench	ST003869
RNA-seq from proliferating and senescent IMR90 fibroblasts	Gene Expression Omnibus (GEO) public available	GEO: GSE61130
RNA-seq from replicative senescence mitoplasts	Gene Expression Omnibus (GEO) public available	GEO: GSE73458
H3K79Succ peaks	Gene Expression Omnibus (GEO) public available	GEO: GSE97994
Experimental models: Cell lines		
IMR90	ATCC	ATCC-CCL-186
HEK-293T	ATCC	ATCC-CRL-3216
TIG3 hTERT pMSCV-ER:ΔBRAF	Kindly provided by Dr. Lund's laboratory(BRIC, COPENHAGEN, DK)	N/A
COV362	SIGMA	1VL-7071910
Oligonucleotides		
List of primers for qPCR and for cloning listed in Supplementary Tabl 5	Condalab	N/A
siRNA_CTRL	SIGMA-MERCK	CAGUCGCGUUUGCGACUGGCdTdT
siRNA sin-lncRNA#1	SIGMA-MERCK	GGAUGUUCCUGUUGGUCCAdtdt

(*Continued on next page*)

Continued

REAGENT or RESOURCE	SOURCE	IDENTIFIER
siRNA sin-lncRNA#3	SIGMA-MERCK	CGGAGAGACCAUUCACUCAdtdt
siRNAC/EBPb	SIGMA-MERCK	GGUCUUUUUUUGUAUUAUAdtdt
siRNA DLST	SIGMA-MERCK	UAGCUUCCACAUUCCUGAUGACUGGdTdT
Recombinant DNA		
pLTVX-WT-DLST	Generated in this work	N/A
pLTVX-Mut-DLST (R224A/K226E)	Generated in this work	N/A
pLVX-TetOne Puro Vector	Takara	631847
pcDNA3.1(+) plasmid		N/A
lentiCRISPRv2	Kindly gift by Dr. Agami's lab (NKI, Amsterdam)	#5296113 Adgene
pLNCX-ER:RAS	Kindly provided by Dr. Gil's lab (ICL, London)	N/A
Software and algorithms		
ImageJ		2.14.0/1.54f
GraphPad Prism		v10
BOWTIE2 algorithm		v.2.1.0
Image Lab	Biorad	N/A
QuantStudio		N/A
Image Studio Lite	Odyssey	version 5.2
BD FACSDiva v 8.0.1	BD Bioscience	N/A
R bioconductor		N/A
Zen software	Zeiss	Version 2012

EXPERIMENTAL MODEL AND STUDY PARTICIPANT DETAILS

Cells

IMR90 lung fibroblasts and HEK-293T cells were purchased from ATCC. TIG3 hTERT pMSCV-ER:ΔBRAF lung fibroblasts[33] were kindly provided by Dr. Lund's laboratory (BRIC - Copenhagen, Denmark). All cell lines were cultured in DMEM medium (GIBCO), supplemented with 10% fetal bovine serum (GIBCO) and 1x penicillin/streptomycin (GIBCO). Cells were maintained at 37 °C in the presence of 5% CO2 and tested for mycoplasma contamination regularly, using the MycoAlert Mycoplasma Detection Kit (Lonza).

COV362 cells were obtained from SIGMA, kindly provided by Dr. Beatriz Tavira (CIMA) and cultured in DMEM medium (GIBCO), supplemented with 10% fetal bovine serum (GIBCO) and 1x penicillin/streptomycin (GIBCO).

To generate OIS cell systems, viruses were first produced in HEK-293T cells transfected with 12μg of either pLNCX-ER:RAS or pLNCX (Empty) vectors, 6μg of gag-pol plasmid, 3μg of pVSVG vector and 1μg of pMAX-GFP plasmid (to check transfection efficiency). Transfection reaction was carried out in opti-MEM medium (GIBCO) using Lipofectamine 2000 (Invitrogen), following manufacturer's instructions. 48 h after transfection, filtered supernatant supplemented with 4 μg/ml polybrene (Santa Cruz), was used to transduce low passage IMR90. Cells were selected with Neomycin-G418 (Sigma) at a final concentration of 400 μg/ml for at least one week.

pLTVX-WT-DLST or pLTVX-Mut-DLST (R224A/K226E) cell lines were generated by lentiviral infection. HEK293T cells were transfected using Lipofectamine 2000 (Life Technologies) with 7 μg of pLTVX-WT-DLST or pLTVX-Mut-DLST (R224A/K226E), together with 6 μg of VsVg and 5 μg Pax8 viral plasmids. After 48 h, supernatants containing the viral particles were filtered through a 0.45-μm filter. Confluent IMR90 ER:RAS cells were then infected with one-third of the viral supernatant and 8 μg/μL polybrene. Twenty-four hours post infection, the cells were selected with 1 μg/μL puromycin. Cells were maintained in tetracycline-free tested serum (Clontech). For the expression of the protein 100 ng/mL doxycicline was used for 72 h.

METHOD DETAILS

Senescence induction and cell treatments

For senescence induction studies, IMR90 ER:RAS or TIG3-hTERT ΔER:BRAF fibroblasts have been treated with 200nM of 4-hydroxy-tamoxifen (4OHT) for three days unless specified otherwise in the text. When longer time courses were needed, medium was replaced on day 3. Only normal fibroblasts cell lines with less than 20–25 passages were used for experiments.

For senescence induction the cells were treated with 10 μM cisplatin for 10 days.
N-Acetyl-L-cysteine (NAC, SIGMA) was added at 5 mM 1h prior 4-OHT treatment and for the duration of the experiment.

Irradiation

To induce senescence by ionizing radiation, IMR90 cells were γ-irradiated at 5Gy and harvested at the indicated times. Radiation was delivered at 180 cGy/min using a Siemens Oncor Impression Plus linear accelerator equipped with 6MeV X-rays.

RNAi studies

For siRNA studies, cells were transfected once with a final concentration of 40nM siRNA using Lipofectamine 2000 (Invitrogen) in opti-MEM medium (GIBCO), unless differently stated in the text. Scrambled siRNA (siRNA CTRL in the text) was used as transfection control. All siRNAs employed in this study were designed using BLOCK-iTTM RNAi Designer (https://rnaidesigner.thermofisher.com/rnaiexpress/) and purchased from Sigma, except C/EBPβ siRNA, a kind gift of Dr. Aragón (CIMA - Pamplona, Spain).

To induce senescence in transfected cells, the transfection medium was replaced after 6 h with complete medium containing 200nM 4OHT. When a senescence induction longer than 3 days was needed, transfected cells were trypsinized and re-plated to perform multiple analyses in parallel. All siRNAs used in this study are listed in Table S8.

CRISPR-Cas9 gene editing

The CRISPR Design Tool from the Zhang Lab (http://crispr.mit.edu/) was used to find suitable target sites for the Streptococcus pyogenes Cas9 (SpCas9) in *sin-lncRNA* genomic region. Specific guide RNAs (sgRNA_up and sgRNA_dw (see Table S7), were cloned into the lentiviral plasmid lentiCRISPRv2 carrying spCas9 gene and puromycin resistance, a kind gift from Dr. Agami's lab (NKI - Amsterdam, Netherlands) and originally generated in Dr. Zhang's lab (for details, see plasmid reference #5296113 on Addgene website).

LentiCRISPR vectors carrying the two independent sgRNAs were separately transfected in HEK-293T cells to generate viral particles, as described above. LentiCRISPR viruses were mixed (ratio 1:1) and used to transduce TIG3-hTERT ΔER:BRAF fibroblasts, then selected with 1 μg/ml of puromycin. Single puromycin-resistant TIG3 cells were sorted in 96-well plates, using untreated TIG3 fibroblasts as feeder cells, which were then eliminated by a second round of puromycin selection (0.5 μg/ml). Genomic DNA was isolated from puromycin-resistant clones using QuickExtract DNA extraction solution (Lucigen), PCR amplified and tested on agarose gel for accurate deletion.

Cell proliferation assays

For crystal violet assay upon OIS, 1-2×10^4 untreated or transfected cells were plated in 6-well plates and senescence induction was prolonged for 5 days in 4-OHT medium. Cells were fixed with 0.5% glutaraldehyde for 15 min and stained with 0.1% Crystal Violet solution (Sigma) for 30 min. To quantify cell density, cells were incubated with 500μL of 10% acetic acid (Sigma) and collected in ELISA plates. Absorbance was measured by spectrophotometry at 570 nm in a SPECTROstar Nano equipment.

For BrdU incorporation assay, cells were labeled with 50 μM BrdU solution (BD Pharmingen) for 16–18 h. In case of senescent cells, OIS was previously induced for 5 days before starting BrdU assay. Then, cells were harvested by trypsinization and BrdU staining was performed using BrdU Flow Kits (BD Pharmingen), according to manufacturer's instructions. Amount of BrdU incorporation was measured by flow cytometry using a FACSCalibur Cell Analyzer (BD Bioscience).

Apoptosis staining

Apoptosis was measured using BD Pharmingen PE Annexin V Apoptosis Detection Kit I (BD Bioscience). Briefly, cells were washed twice with cold PBS and then resuspend cells in 1X Binding Buffer at a concentration of 1 x 10°6 cells/ml. 1 x 10°5 cells were stained with 5 μL of PE Annexin V and 5 μL 7-AAD. After 15 min incubation at RT in the dark. 400 μL of 1X Binding Buffer was added to each tube. Apoptosis levels were measured by flow cytometry using a FACSCalibur Cell Analyzer (BD Bioscience).

SA-β-gal staining

To detect SA-β-gal activity, 1×10^3 of untreated or transfected cells were plated in 6-well plates and senescence was induced for 8 days upon 4-OHT treatment. Cells were fixed with 0.5% glutaraldehyde solution for 15 min at RT and washed with PBS containing 1mM MgCl2 (pH 6.0). Then, cells were incubated overnight at 37 °C in X-gal staining solution (1 mg/ml X-gal [Thermo Fisher], 0.12 mM K3Fe(CN)6 [Merk], 0.12 mM K4Fe(CN)6 [Merk], PBS/MgCl2 [pH 6.0]). Alternatively, the SA-β-gal staining kit (Cell signaling technology). Cells were washed and percentage of blue cells was counted manually using an inverted microscope.

ROS/RNS measurement assay

Senescent IMR90 ER:RAS fibroblasts transfected with *sin-lncRNA* targeting or control siRNAs were collected by trypsinization and re-suspended at 0.5–1×10^6 cells/ml in Hypotonic Buffer (10mM Tris HCl [pH 7.5], 10mM NaCl, 1.5mM MgCl2). To facilitate membrane lysis, cells were incubated for 10 min at 4 °C and sonicated for 5 cycles (30″ON-30″OFF) in a Bioruptor sonication device. Cell extract was cleared by centrifugation and assayed for ROS/RNS accumulation by fluorescence-based approach using

OxiSelect *in vitro* ROS/RNS Assay Kit (Cell Biolabs), following manufacturer's instructions. The amount of fluorescent oxidized probe (2′, 7' -dichlorodihydrofluorescein or DCF) was measured with a fluorescence plate reader at 480nm excitation/530nM emission. Data were interpolated to a DCF standard curve to obtain absolute values.

Oxygen consumption rate and extracellular acidification

Cellular OCR was measured using a Seahorse XF Cell Mito Stress Test and a Seahorse Bioanalyzer XFe96 (Agilent Technologies) according to the manufacturer's standard protocol. Briefly, 200,000 IMR90 cells were reverse transfected with the corresponding siRNAs in 6 well plates. After 24h cells were treated with 500 nM 4-OHT. After 3 days of treatment, cells were trypsinized and seeded on Seahorse XF96 Cell Culture microplates to confluence (10000 cells/well) and were subjected to metabolic profiling the next day. For Mito stress tests, cells were cultured for 1 h in a CO_2-free incubator at 37°C. Oxygen consumption rates (OCR) were monitored at basal conditions and, after sequential injections of 1 μM oligomycin to block the mitochondrial ATP synthase, 1.5 μM FCCP to uncouple oxidative phosphorylation, 1 μM antimycin A and 1 μM rotenone were used to fully inhibit mitochondrial respiration and 50 mM 2-deoxyglucose (2-dG) to block glycolysis. Two separate measurements of OCR and extracellular acidification rate (ECAR) from 4 independent experiments were taken after the addition of each inhibitor. Samples were normalized based on the protein concentration. All reagents were purchased from Agilent Technologies.

Lactate measurements

IMR90 ER:RAS fibroblasts were transfected with *sin-lncRNA* targeting or control siRNAs and treated with 4-OHT for 6 days. The supernatant was harvested and centrifuged for 5 min at 500 g. Lactate levels were measured using Cobas C311 Analyzer with LACT2 kits (Roche Diagnostics GmbH). Human Precinorm y Precipath were used as controls.

Liquid chromatographic -mass spectrometry (LC-MS) metabolomics

Isotope labeling

6-day senescent IMR90 ER:RAS fibroblasts transfected with siRNA control or siRNA against *sin-lncRNA* or DLST were incubated with glutamine-free DMEM supplemented with 4 mM L-$^{13}C_5$-Glutamine (Cambridge Isotopes Laboratories). After 6 h the cells were washed with PBS 1x and snap-freeze in liquid nitrogen.

Sample preparation and LC/MS methods

LCMS was performed at the Metabolomics Platform at CIC bioGUNE (Donostia, Spain). Cells from three wells (1E6 cells/well) were pooled to obtain one LCMS sample. Therefore, cells were extracted with 200 μL icecold extraction liquid per well. The volume from one well was transferred to the next and finally the resulting 600 μL volume was passed over the three wells two times. The extraction liquid consisted of a mixture of ice-cold methanol/water (50/50 %v/v). Subsequently 400 μL of the cell homogenate plus 400μL of chloroform was transferred to a new aliquot and shaken at 1400 rpm for 60 min at 4°C. Next the aliquots were centrifuged for 30 min at 14000 rpm at 4°C. 250μL of the aqueous phase was transferred to a fresh aliquot. The chilled supernatants were evaporated with a speedvac in approximately 2h. The resulting pellets were resuspended in 150 μL water/MeOH (75/25 %v/v). Samples were measured with a UPLC system (Acquity, Waters Inc., Manchester, UK) coupled to a Time-of-Flight mass spectrometer (ToF MS, SYNAPT G2S, Waters Inc.). A 2.1 × 100 mm, 1.7 μm Phenyl-Hexyl column (Waters Inc.), thermostated at 40°C, was used to separate the analytes before entering the MS. Mobile phase solvent A (aqueous phase) consisted of 99.5% water and 0.5% FA while solvent B (organic phase) consisted of 99.5% MeCN and 0.5% FA. In order to obtain a good separation of the analytes the following gradient was used: from 98% A to 0% A in 2 min in curved gradient (#8, as defined by Waters), constant at 0% A for 1 min, back to 98% A in 0.2 min. The flow rate was 0.250 mL/min and the injection volume was 3 μL. After every 6 injections, a sample was injected. The MS was operated in negative electrospray ionization in full scan mode. The cone voltage was 10 V, cone offset was 50V and capillary voltage was 400 V. Source temperature was set to 120°C and capillary temperature to 500°C. The flow of the cone, desolvation and nebulizer gas (nitrogen) were set to 5 L/h, 6 L/h and 850 L/h, respectively. A 2 ng/mL leucine-enkephalin solution in water/acetonitrile/formic acid (49.9/50/0.1 %v/v/v) was infused at 10 μL/min and used for a lock mass which was measured each 36 s for 0.5 s. Spectral peaks were automatically corrected for deviations in the lock mass. Extracted ion traces for relevant analytes were obtained in a 10 mDa window in their expected *m/z*-channels. These traces were subsequently smoothed and peak areas integrated with TargetLynx software. Signals of labeled analytes were corrected for naturally occurring isotopes. Since we also had unlabeled experiments, for some metabolites we could determine the naturally occurring isotope-distribution empirically. This was necessary for the first and second isotopomers since correcting with theoretical values did not eliminate these isotopes from unlabeled experiments. This is probably because signals are non-linear with respect to ion-counts, i.e., higher ion-counts tend to have *relatively* lower signals than lower ion-counts due to saturation of the detector. The calculated raw signals were adjusted by median fold-change (MFC) adjustment. This is a robust adjustment factor for global variations in signal due to e.g., difference in tissue amounts, signal drift or evaporation. The MFC is based on the total amount of detected mass spectrometric features (unique retention time/mass pairs). The calculations and performance of the MFC adjustment factors are described in the following publications.[82,83]

Immunofluorescence and RNA fluorescence *in situ* hybridization (RNA-FISH)

For fluorescence-based studies, IMR90 ER:RAS cells were collected by trypsinization after required treatments (as specified in the text) and re-plated on top of cover glasses placed on clean 6-well plates. The following day, cells were washed and fixed for 15 min at room temperature (RT) using 3% methanol-free formaldehyde solution (Thermo Fisher).

For immunofluorescence studies, fixed cells were washed (PBS/0.5% NP-40) and incubated first with block solution (10% FBS in wash buffer) for 20 min and then with primary antibody diluted in block solution for 1 h at RT. Antibody solution was washed out and cells were incubated with fluorophore-conjugated secondary antibody for 30 min. After extensive washes, cover glasses were mounted on microscope slides using DAPI-containing mounting solution (Palex Medicals) and pictures were collected with an automated optical microscope running Zen 2 core imaging software (Zeiss), according to standard procedures.

For RNA-ISH studies, fluorescein-labeled Locked Nucleic Acid (LNA) DNA probes were designed and synthesized by Exiqon and were hybridized according to manufacturer's protocol with some modifications. Briefly, fixed cells were first incubated with 70% ethanol for 1 h and then with Acetylation Buffer (0.1M Triethanol Amine, 0.5% (v/v) Acetic Anhydride) for 30 min at RT. To avoid non-specific probe binding, cells were incubated with Hybridization buffer (10% dextran sulfate, 50% formamide, 2x saline sodium citrate [SSC] buffer) for 1 h at 55°C. Specific LNA probes were denatured at 92°C for 4 min and then mixed with Hybridization buffer at a final concentration of 20nM. Hybridization was carried out overnight at 55°C. The following day, probes residues were eliminated using 2x SSC wash buffer and fixed cells were treated with 3% Hydrogen Peroxide for 30 min at RT. For fluorescein (FAM) detection, cells were first incubated 1 h with Blocking Buffer (10% heat-inactivated Goat Serum, 0.5% Blocking Reagent [Roche] in PBS-0.5% Tween) and then 1 h with 1.5U/ml αFAM-POD antibody (Roche) diluted in Blocking Buffer. After extensive washes, fluorescent signal was developed by 10 min incubation with TSA-Cy3 solution (PerkinElmer). Residues were eliminated through stringent 4x SSC washing and slides were prepared for microscope detection using DAPI mounting solution, as mentioned above.

Slides were imaged on a fluorescence inverted microscope using a 63× objective. At least 10 optical stacks were acquired per image for DAPI (nuclear stain) and for the fluorescence channel corresponding to the RNA FISH probe (Cy3). Image processing was performed using Zen software (version 2.3 - Zeiss) and for each condition, signal was adjusted on a sample incubated with no probes and used as control for background detection. ImageJ software was employed for stacks deconvolution.

Protein extraction and immunoblot analysis

Cells were lysed for 15 min in rotation at 4°C using RIPA buffer (150mM NaCl, 25mM Tris HCl [pH 7.5], 2mM EDTA, 0.1% sodium deoxycholate [Na-DOC], 0.1% SDS, 1% Triton X-100) supplemented with 1x cOmplete Protease Inhibitor Cocktail [Roche]. For detection of phosphoproteins, 1x PhosSTOP phosphatase inhibitor [Roche] was freshly added to RIPA solution. Lysed cells were centrifuged at max speed for 10 min at 4°C and the insoluble pellet was discarded. Protein concentration was estimated by Pierce BCA Protein Assay Kit, using BSA curve as reference and according to manufacturer's instructions. Proteins were separated on denaturing SDS-PAGE gels and transferred to a nitrocellulose membrane [Biorad] following standard procedures. Membranes were blocked using skim milk or BSA (VWR) and probed first for primary and then for HRP-conjugated secondary antibody. Western Lightening ECL- Plus (PerkinElmer) was employed for chemiluminescence detection of proteins. The list of antibodies used in this study can be found in Table S9.

Cellular fractionation

IMR90 cells were reverse transfected with control or siRNA 1/3 *sin-lncRNA*. The day after transfection cells were treated with 500 nM 4-OHT for 5 days. Cells were scrapped in cold PBS and centrifuge 5 min 0.2g. Pellets were resuspended in NIB buffer (1.28 M Sucrose, 40 mM Tris pH 7.4, 20 mM MgCl2, 4% Triton X-100), incubated on ice for 20 min and centrifuged 15 min at 2500rpm. The supernatant was kept as the cytosolic fraction and further cleaned by an extra centrifugation step. Nuclear pellets were washed twice with NWB (40 mM Tris pH 7.4, 20 mM $MgCl_2$) by centrifugation 15 min at 2500 rpm. RIPA (150 mM NaCL, 25 mM Tris pH 8, 0.1% SDS, 0.1% Na-Deoxycholate, 2 mM EDTA, 1% Triton X-100) buffer was used to lyse the nuclei. After 10 min centrifugation at max speed the supernatant was isolated as the nuclear fraction. Immunoblot analysis was performed as described above.

Mitochondria isolation

10 cm plates of senescent cells were incubated with 200nM of MitoTracker for 30 min (Invitrogen). Cells were collected by trypsinization and resuspended in 1mL of PBS. Cells were lysed using by 20 strokes up and down using a 2 mL cell douncer. After 5 min centrigfugation at 700 g at 4°C the supernatant was collected. Mitochondria were pellet by centrifugation at 12,000g for 5 min at 4°C, washed with PBS once and resuspended in 200 mL of filtered PBS. Mitochondria were purified by FACS sorter using Flow Cytometry Size Calibration Kit (Invitrogen).

Native RNA immunoprecipitation

20×10^6 cells were collected in cold PBS by scraping and lysed in RIP buffer (25 mM Tris-HCl pH 7.4, 150 mM KCl, 5mM EDTA, 0.5% Nonidet P-40, 20 U ml^{-1} RNAsin (Promega), 0.5 mM dithiothreitol (DTT) and 1× protease inhibitor mixture Complete (Roche)). After centrifugation, the samples were precleared with Dynabeads Protein A (Invitrogen) for 1 h. One per cent of the sample was used as the input control and the remaining extracts were incubated with 10 μg DLST antibody (Bethyl) or IgG at 4 °C overnight. RNA–antibody complexes were collected by incubation with Dynabeads Protein A. After extensive washing in RIP buffer (25 mM

Tris-HCl pH 7.4, 150 mM KCl, 5mM EDTA, 0.5% Nonidet P-40, 20 U ml^{-1} RNAsin (Promega), 0.5 mM dithiothreitol (DTT) and 1× protease inhibitor mixture Complete (Roche)), 1/5 of the sample was used for western blotting control and the remaining for RNA extraction and qRT–PCR analysis, as described below.

In vitro RNA pulldown

RNA pulldown was performed according to.[84] Briefly, biotin-labeled *sin-lncRNA* and control RNA (cloned in a pcDNA3.1(+) plasmid) were generated *in vitro* using T7 or T3 RNA polymerase, respectively (Applied Biosystems). The fragments used for the mapping were *in vitro* transcribed from PCR products carrying the sequence of the T7 promoter in the forward primer (Table S7). Biotinylated RNAs were treated with RNase-free DNase I (Promega), purified on G-50 MicroSpin columns (GE Healthcare) and heated to 65°C for 10 min and cooled down slowly to 4°C to allow proper RNA folding. 10×10^6 IMR90 ER:RAS were collected after 6 days of senescence induction and total protein extracts were prepared using RIPA buffer. Cell extracts were then incubated with 10 μg of biotinylated RNA in Buffer A (150mM KCl, 25mM Tris pH 7.4, 5mM EDTA, 0.5mM DTT, 0.5% NP40) supplemented with fresh protease inhibitors and yeast tRNA (0.1 μg/ml) and rotated overnight at 4C. Dynabeads MyOne Streptavidin T1 beads (Invitrogen) were used to isolate RNA-protein complexes. Beads were washed 5 times in buffer A (150 mM KCl, 25 mM Tris pH 7.4, 5 mM EDTA, 0.5 mM DTT, 0.5% NP40, 1x protease inhibitor cocktail (Roche), 1 mM PMSF, 100 U/ml SUPERASin) and boiled in 2X Laemmli loading buffer, and retrieved proteins were loaded in a NuPAGE 4%–12% bis-Tris gel (Invitrogen). Gel was stained with the SilverQuest Silver Staining Kit (Thermo Fisher) to identify differential bands comparing *sin-lncRNA* and control RNA samples. We isolated a band of ~50–55 kDa unique for *sin-lncRNA* (Figure S5). Unique bands were cut and submitted for Mass Spectrometry (MS) analysis to the Taplin MS Facility (Harvard University).

For the mapping of the fragments, the pull down was done as indicated above but cisplatin-induced senescence COV362 cells were used.

Chromatin immunoprecipitation (ChIP)

10×10^6 cells were crosslinked with 1% formaldehyde for 10 min at RT and nuclei were isolated with cell lysis buffer (5mM Tris pH8.0, 85mM KCl, 0.5% NP40, supplemented with fresh 0.5 mM DTT and 1× protease inhibitor mixture Complete (Roche)). Nuclear pellet was then resuspended in RIPA buffer (1X PBS, 1% NP40, 0.5% Na-deoxycholate, 0.1% SDS, supplemented with 1× protease inhibitor mixture Complete (Roche)) and chromatin was sheared to a range of 200–500 bp by using a Bioruptor instrument (Diagenode) with the following settings: 8 cycles LOW, 30″ON/30″OFF. Sonicated chromatin was incubated overnight with 6μg of C/EBPβ, H3K79Succ or IgG antibody (listed in Table S6).) followed by 2h incubation with Dynabeads Protein G beads (Invitrogen). After five washes with LiCl buffer (100mM Tris pH 7.5, 500mM LiCl, 1% NP40, 1% Na-deoxycholate) and TE buffer, DNA was reverse crosslinked by incubating beads in Elution buffer (1% SDS, 0.1M NaHCO3 and Proteinase K (NEB)). C/EBPβ and H3K79Succ binding was analyzed by qPCR using specific primers (Table S6).

RNA extraction and RT-qPCR analysis

Total RNA was isolated using TRI reagent (Sigma), treated with DNase I (Invitrogen) and reverse-transcribed using the High-Capacity cDNA Reverse Transcription Kit (Applied Biosystem) with random hexamer primers following manufacturer's instructions. The obtained cDNA was analyzed by quantitative PCR using iTaq Universal SYBR Green supermix (Bio-Rad) in a ViiATM 7 Real-Time PCR System machine (Thermo-Fisher). All reactions were performed in triplicate or quadruplicate and HPRT1 (Hypoxanthine Phosphoribosyl transferase 1) RNA levels were used for normalization, unless specified otherwise in figure legend.

To calculate the number of *sin-lncRNA* molecules per cell, *sin-lncRNA* cloned in pcDNA3.1 vector was *in vitro* transcribed, quantified and converted to number of copies based on its predicted molecular weight. Dilutions of this transcript were retro-transcribed and used as standard curve for qPCR analysis along with cDNA obtained from a precise number of IMR90 proliferating or senescent cells. All qPCR primer sequences are provided in Table S5.

RNA sequencing and data analysis

Raw data of Poly-A+ RNA-seq from proliferating and senescent IMR90 fibroblasts were kindly provided by Dr. Gil's laboratory (Imperial College London, UK) before their publication and are now available at the Gene Expression Omnibus under the accession number GSE61130.[28] For RNA-seq of IMR90 ER:RAS fibroblasts treated with sin-lncRNA or control siRNA, cells were transfected and 4OHT-treated for 3 days, as described above. Total RNA from samples prepared in biological triplicate was isolated with TRI reagent, purified and treated with DNAse I using RNAeasy mini-Kit (Qiagen). After quality evaluation by Experion kit and quantification by Qubit, 1μg of RNA was used for library preparation and sequenced on Illumina HiSeq 2000 (33×10^6 reads per sample, 50bp single-end sequencing modality). Sequenced reads from three different replicates were aligned to hg19 genome using the BOWTIE2 algorithm (v.2.1.0) was used to quantify the number of reads in annotated genes[85,86] To identify enriched molecular pathways associated with differences in gene expression, Gene Set Enrichment Analysis (GSEA, Broad Institute, http://www.broadinstitute.org/gsea/index.jsp) was performed using the Hallmark gene sets in the Human MSigDB database.[87] Enriched pathways were selected with Normalized Enrichment Score (NES) >±1 and adj.Pvalue<$1e^{-4}$.

Sin-lncRNA expression analysis in tumor samples

TCGA RNA-seq expression data was retrieved using R bioconductor library TCGA biolinks, and represented using R.

QUANTIFICATION AND STATISTICAL ANALYSIS

Unless specified otherwise, experimental data were represented as mean ± standard deviation of at least three biological replicates (unless otherwise stated in figure legends) and significance was determined by two-tailed unpaired or Student's t-test or one sample using GraphPad software. Data are presented as the mean ± SD. ns, not significant. $^{*}p < .05$; $^{**}p < .01$; $^{***}p < 0.001$.